

THESIS FOR THE DEGREE OF DOCTOR OF PHILOSOPHY

Miniaturized localized surface plasmon resonance biosensors

SI CHEN

Department of Applied Physics
CHALMERS UNIVERSITY OF TECHNOLOGY
Göteborg, Sweden 2013

Miniaturized localized surface plasmon resonance biosensors

Si Chen

ISBN 978-91-7385-851-9

© Si Chen, 2013.

Doktorsavhandlingar vid Chalmers tekniska högskola
Ny serie nr 3532

ISSN 0346-718X

Department of Applied Physics
Chalmers University of Technology
SE-412 96 Göteborg
Sweden
Telephone + 46 (0)31-772 1000

Cover: Up left, a photograph of a droplet of water on the surface of gold nanostructures supported on glass and a droplet of water on the surface of a thin gold film. Down left, a photograph of a single nanoparticle array of gold nanorod prepared by electron beam lithography. Up right, single nanoparticle scattering spectra. Down right, schematic for ELISA enhanced plasmonic sensing.

Göteborg, Sweden 2013

Miniaturized localized surface plasmon resonance biosensors

SI CHEN

Department of Applied Physics
Chalmers University of Technology

Abstract

Reliable and sensitive biosensors are required for fast and accurate diagnostics. Localized surface plasmon resonances (LSPRs) in noble-metal nanoparticles possess very high refractive index sensitivity close to the metal surface and therefore constitute an attractive biosensing platform. In this thesis, label-free biosensing with LSPR was investigated and demonstrated. The spatial sensing ranges of the particles were determined by thin layer deposition of dielectric materials. A comparison between the classical SPR and LSPR was performed using the same experimental setup. No obvious performance difference between the two sensing techniques was found. The versatility of the LSPR sensing technique was demonstrated by miniaturization of the sensor area, which could be reduced down to ~250 nanoparticles without compromising the short-term noise level.

To further miniaturize the LSPR sensor, multiple single nanoparticles were measured using hyperspectral imaging. It was shown that by combining LSPR refractive index sensing and an enzyme linked immunoassay (ELISA), i.e. a horseradish peroxidase catalyzed precipitation, an extremely low surface coverage of enzyme molecules could be detected on single isolated nanoparticles. In a follow up investigation, electron beam lithography (EBL) and hyperspectral imaging were combined to enable simultaneous measurements of up to 700 individual particles. This made it possible to study statistical variations between the sensor particles. The observed variations in the responses from individual particles were interpreted as a result of large variations in sensitivity over the particle surface combined with the size distribution of the precipitate.

In a separate study, a photo functionalization strategy compatible with LSPR biosensors was investigated. A biotin moiety was successfully functionalized with UV light on a self-assembled monolayer of photoactive nitroindoline on gold surfaces. Adsorption of streptavidin and streptavidin conjugated HRP to the surface-bound biotin could be monitored by the LSPR sensor. This strategy might be utilized for spatially localized surface functionalization for multiplexed miniaturized LSPR sensors.

In summary, despite many experimental problems, the results discussed in this thesis point towards a number of important biosensing applications of plasmonic nanoparticles.

Keywords: Surface plasmon resonance, biosensing, single molecule, hyperspectral imaging, photo functionalization, colloidal lithography, electron beam lithography

LIST OF PUBLICATIONS

This thesis is based on the work contained in the following papers, referred to by Roman numerals in the text:

I. Ultrahigh sensitivity made simple: nanoplasmonic label-free biosensing with an extremely low limit-of-detection for bacterial and cancer diagnostics

S. Chen, M Svedendahl, M Käll, L Gunnarsson and A Dmitriev

Nanotechnology, 2009, 20, 434015-434024

II: Refractometric Sensing Using Propagating versus Localized Surface Plasmons: A Direct Comparison

M. Svedendahl, S. Chen, A. Dmitriev, M. Käll

Nano Letters, 2009, 9 (12), 4428-4433

III: High-Resolution Microspectroscopy of Plasmonic Nanostructures for Miniaturized Biosensing

A. Dahlin, S. Chen, M. P. Jonsson, L. Gunnarsson, M. Käll and F. Höök

Analytical Chemistry, 2009, 81 (16), 6572-6580

IV: Plasmon-Enhanced Colorimetric ELISA with Single Molecule Sensitivity

S. Chen, M. Svedendahl, R. P. Van Duyne, M. Käll

Nano Letters, 2011, 11 (4), 1826-1830

V: Towards Plasmonic Biosensors Functionalized by a Photo-Induced Surface Reaction

T. A. Gschneidner, S. Chen, J. B. Christensen, M. Käll, K. Moth-Poulsen

(submitted to Journal of Physical Chemistry C)

VI: ELISA enhanced LSPR sensing on large arrays of single particles prepared by electron beam lithography

S. Chen, M. Svedendahl, T. Antosiewicz, M. Käll

(in manuscript)

My contributions:

I: I planned the experiments, fabricated samples for the sensing experiments and wrote the first draft of the paper.

II: I fabricated the samples, participated in designing the experiments and in the discussion and analysis of the results.

III: I fabricated samples for the experiments and participated in the discussion of the results.

IV: I initiated the project, designed the experiments and wrote a draft of the manuscript.

V: I planned the surface chemistry experiments, fabricated sensors and performed the biosensing experiment on the plasmonic surface. I also wrote part of the manuscript and the discussion

VI: I built the experimental setup, fabricated samples and performed experiments. I also wrote a draft the manucrypt.

Works not include in this thesis

I: A bimetallic nanoantenna for directional colour routing

T. Shegai, S. Chen, V. D. Miljković, G. Zengin, P. Johansson and M. Käll

Nature Communication, 2011, 2, 481-487

II: Metal nanoparticles amplify photodynamic effect on skin cells in vitro

B. Bauer, S. Chen, M. Käll, L. Gunnarsson, M. B. Ericson

Proc. SPIE 7897, Optical Interactions with Tissue and Cells XXII, 789712

II: Enhanced Nanoplasmonic Optical Sensors with Reduced Substrate Effect

A. Dmitriev, C. Hägglund, S. Chen, H. Fredriksson, T. Pakizeh, M. Käll and D. S. Sutherland

Nano Letters, 2008, 8 (11), 3893-3898

Contents

Chapter 1 Introduction.....	1
Chapter 2 Molecular interactions	5
Langmuir isotherm	5
Reaction time associated with biosensors	6
Chapter 3 Introduction to plasmonic based refractive index sensors.....	11
Introduction to plasmonics.....	11
Localised surface plasmon resonance.....	13
Biosensing with plasmons	15
Chapter 4 Fabrication of nanoparticles.....	21
Hole mask colloidal lithography.....	21
Electron beam lithography.....	23
Chapter 5 Schemes of measurement and analysis	25
Optical measurements.....	25
Micro extinction and dark field measurements.....	26
Single particle spectral imaging and image analysis.....	27
Chapter 6 Surface chemistry and biomolecules	33
HRP enzymology.....	33
Self-assembled monolayers	35
Streptavidin and biotin.....	35
Photochemistry and photofunctionalization	37
Chapter 7 Summary of appended papers and outlook	39
Future works	41
Acknowledgements	42
References	43

Chapter 1 Introduction

In our daily life, we encounter many sensors of different types every day. When we approach the exit, the door opens itself. When a fire starts, the smoke detector rings. A biosensor is a specific type of sensor that reports the status and interactions of biological matter. The earliest biosensor was probably the Canary bird that coal miners brought down in the mines for early detection of poisonous gas. The Canary bird is more sensitive towards gas than humans therefore gives the miners an early warning of the danger. Among modern biosensors, the most well-known is probably the pregnancy home test, which detects increased levels of human chorionic gonadotropin (hCG) as an indication of pregnancy.

The term 'biosensor' refers to a vast collection of different methods that are all based on the central dogma illustrated in Figure 1-1. A biosensor is thus composed of four principle components: the medium that carries the analytes of interest; selective capturing agents; a signal transducer and read out component. The medium could take many forms, such as water, gas or some complex body fluid, for example blood. The capturing agents can also take many forms, such as single stranded DNA, antibody or antigen. The main function of the capturing agent is to concentrate the analyte on the surface of the transducer. This usually relies on a specific interaction between the capturing agent and the analyte.

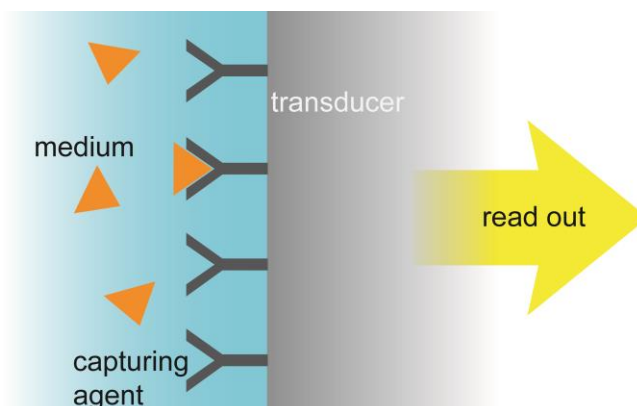


Figure 1-1. There are normally four different components in a biosensor: the medium that carries the target molecule, the capturing molecules on the surface of the signal transducer, the transducer and the read out system that detects the change in transducer signal upon binding of the target molecules to the surface.

There are many types of transducers based on detecting different changes of physical properties. The sensor could be based on a change in conductivity upon interaction with the target molecules,¹ a change of weight, as in the case of the quartz crystal microbalance² and the micro cantilever,³⁻⁴ or changes in refractive index from the analytes interaction with the transducer, as in ellipsometry⁵ and plasmon based sensors.⁶⁻⁸ The focus of this thesis is biosensor transducers based on surface plasmonic resonance (SPR). In 1982, Nylander et al. demonstrated refractive index sensing with plasmons on a thin gold film for the first time and this marked the start of SPR based biosensor development.⁹⁻¹⁰

Localized surface plasmon resonance (LSPR) sensing, a special type of SPR sensing based on nanostructures, was utilized for biosensing for the first time by Englebienne et al. in 1998.¹¹ The huge current interest in nanotechnology and nano-sized biosensors is partly due to the fact that we are now able to fabricate and characterize architectures of that regime, but one also hope that research in nanoscience will result in completely new sensing methods and applications.

The development of biosensors has huge application potential in several fields. One of the most important applications is sensitive diagnostic devices. Novel nanoplasmonic biosensors could potentially be used to complement central diagnostics labs and perhaps be used as point-of-care devices to reduce the response time for diagnostics or for population screening. Plasmon based biosensors have already found many applications in research and industry for studying molecular interactions,^{6,12} for example in the drug discovery industry.

Biosensors that do not require labeling, like QCM, SPR and LSPR, are very powerful tools to study molecular interactions. This is due to several important reasons. The availability of labeled molecules is always an issue. Labeled molecules could be affected by the label itself, which could affect its native interaction strength with the target molecule. Many label free biosensors are also capable to report the kinetics of the interaction by tracking the adsorption in real time, which can directly indicate the binding strength between the molecules. The labeling step can also be labor intensive and expensive.

The most important weakness of the label free techniques is that non-specific binding on the sensor surface will also induce signal change that can be impossible to separate from the specific binding of the target analyte. This has greatly limited the use of label-free biosensors in clinical diagnostic applications, where biomarkers and analytes often exist in low concentrations in media with high concentrations of background molecules.

The limit of detection (LOD) is the minimal detectable signal induced by an amount of molecules per medium volume unit or per sensor surface area unit. A cutoff value of 3 times the noise level is normally considered as an acceptable signal. The detectors in the read out system are usually very sensitive, and good algorithms could extract the information with high accuracy. Therefore the limit of detection is not limited by the noise in the signal, in many cases by signal from unspecific binding from uninteresting molecules that are difficult to separate from the specific binding of the target molecule to the surface of the sensor.

This thesis describes how LSPR can be used as a biosensor. In Chapter 2, different aspects of biosensing will be described. A basic biosensor design principle based on the molecular interaction and diffusion properties will also be discussed. In Chapter 3, the basics of SPR and LSPR sensing are introduced. Fabrication methods used in this thesis is then discussed in chapter 4. Different measurement setups and schemes for surface plasmon resonance sensing used are described in Chapter 5. In Chapter 6, two important molecules used in my work are described in details, namely horse radish peroxidase and nitroindoline. They are utilized for enhancing the sensitivity of the sensor and for photo functionalization of the sensor surface, respectively. In Chapter 7, a short summary of the appended papers and an outlook about the future works is given.

Chapter 2 Molecular interactions

Langmuir isotherm

High sensitivity and low limit of detection is often the most important parameters of a biosensor. The limit of detection is usually given in amount of molecules per volume unit. The interaction between the capturing entities on the transducer surface and the analytes in the reaction chamber is one of the most important processes that determine the limit of detection. A biorecognition reaction such as between an antibody and an antigen or an oligonucleotide hybridization can be written as:

capturing molecule (on the sensor surface) + target molecule (in solution) \leftrightarrow adsorbed molecule

The reaction is reversible and the forward reaction rate (adsorption) is denoted k_{on} while the backward reaction (desorption) k_{off} . The adsorption of target molecule to the surface could be considered as a second order reaction and the desorption as a first orders reaction, in the simplest case. Then the change of surface concentration $\Gamma(t)$ is expressed as:

$$\frac{d\Gamma(t)}{dt} = k_{on}c_0(\Gamma_{max} - \Gamma(t)) - k_{off}\Gamma(t), \quad (2.1)$$

where c_0 is the target molecule concentration in the medium close to the surface. The empty slots available on the surface is denoted as $\Gamma_{max} - \Gamma(t)$, where Γ_{max} is the maximum coverage of the sensor and $k_{off}\Gamma(t)$ is the desorption rate of the molecule from the surface. At equilibrium, $\frac{d\Gamma(t)}{dt} = 0$, the surface coverage is:

$$\Gamma_{eq} = \frac{\Gamma_{max}}{K_D/c_0 + 1}. \quad (2.2)$$

The binding constant K_D denotes the ratio k_{off}/k_{on} . This is the equation that ultimately limits all the surface based biosensors. Except for some “inverse sensitivity” designs, where lower surface coverage gives higher responses the sensor response will increase with the surface coverage Γ .¹³

Reaction time associated with biosensors

The performance of the biosensor is ultimately limited by the surface coverage at the equilibrium. However, the time it takes to reach equilibrium can vary a lot between different affinity pairs. The solution of Eq. (2.1) is:

$$\frac{\Gamma(t)}{\Gamma_{max}} = \frac{k_{on}c_{bulk}}{k_{on}c_{bulk}+k_{off}} \left[1 - \exp\left(-\frac{t}{\tau}\right) \right], \quad (2.3)$$

where $\tau = \frac{1}{k_{on}c_{bulk}+k_{off}}$ is the characteristic time-constant for reaching equilibrium. In order to visualize the time dependence for the different affinity pairs, the surface coverage $\frac{\Gamma}{\Gamma_{max}}$ is plotted for four different reaction times, $t = 1\text{h}$, 5h , 24h and at equilibrium. The values of k_{on} and k_{off} used for the streptavidin-biotin interaction pair was $5 \times 10^6 \text{ M}^{-1}\text{s}^{-1}$ and 10^{-5} s^{-1} . For the antibody case, the k_{on} and k_{off} values for the anti-PSA and PSA was used which are $4 \times 10^4 \text{ M}^{-1}\text{s}^{-1}$ and $4 \times 10^{-5} \text{ s}^{-1}$. For simplicity of analysis, c_0 is for now assumed to be the same as the bulk solution c_{bulk} . For a reaction to reach 95% of the total coverage, the time needed is therefore $t_{95\%} \approx 3 \tau$. For a concentration of 1pM , the $t_{95\%} = 21$ hours for the antibody and antigen pair and for streptavidin and biotin it is 54 hours. The surface coverage $\frac{\Gamma}{\Gamma_{max}}$ is plotted for different concentrations and different reaction times in Figure 2-1, from which we can also read the K_D value at $\frac{1}{2} \Gamma_{max}$ when the system is at equilibrium. It is also easy to see the effect of using a strong affinity pair. At 1 nM concentration and after 1 hour, the antibody-antigen reaction barely results in 10% surface coverage while streptavidin-biotin already give a full coverage.

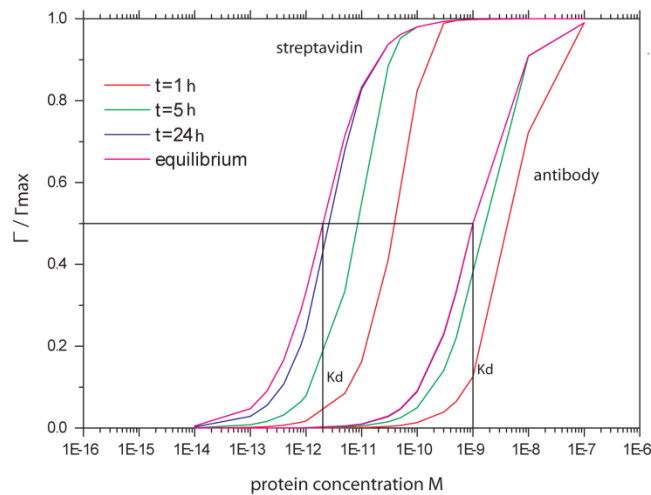


Figure 2-1. Streptavidin-biotin and antibody-antigen surface coverage at different concentrations and times.

The sensors geometric design and liquid handling is an extremely important consideration in biosensing, since it directly affect the sensitivity. In the analysis above, the transport of molecules is assumed instantaneous and, therefore, the concentration at the surface and in the bulk is the same. In reality a depletion layer will quickly forms close to the surface even with microfluidics and continuous injection of molecules to the surface. The effective concentration at the surface will decrease and the molecules from the bulk need to diffuse towards the surface to counter the concentration gradient.

In the following case I will consider the opposite, which is when the reaction rate is instantaneous compared to the diffusion rate of the molecule, so that the reaction is mainly diffusion limited. Sheehan et al¹⁴ has derived an expression for the number of molecules that has passed through the surface of a hemispherical micro or nanoscale sensor after a time t :

$$N(a, t) = 2\pi N_A c_{bulk} D (at + 2a^2 \sqrt{\frac{t}{\pi D}}) \quad (2.4)$$

where N_A is Avogadro's number, D is the diffusion constant for the analyte molecule and a is the radius of the sensor hemisphere. This could be understood as a simulation of diffusion limited reaction for which the reaction rate between the capturing agent and target is infinitely fast and there is no desorption from the surface. It can therefore also be used as an expectation for the absolute maximum number of molecule N that could end up on the surface of the sensor. To show the effect of a miniaturized particle with different concentrations of analyte, equation (2.4) is used to calculate the number of molecules at the surface of a hemispherical sensor with radii between 20 to 100 nm. The diffusion coefficient of the molecules used for the simulation is calculated from the Stokes-Einstein equation:

$$D = \frac{k_B T}{6\pi\eta r} \quad (2.5)$$

where the η is the viscosity of water and r is the radius of the globular streptavidin molecule. For 100 fM to 1 pM concentrations and a sensor radius that varies from 20 nm to 100 nm, the number of molecules that has diffused to the surface after and two hours is show in Figure 2-2. The number of molecules that adsorbed on the surface calculated using the Langmuir isotherm is also shown in the same plot. The value for k_{on} and k_{off} used here is $10^5 M^{-1} s^{-1}$ and $5 \times 10^6 s^{-1}$, similar to the reaction rate between streptavidin and biotin when one of the two is bound to a surface. Γ_{max} , the maximum number of molecules that can be adsorbed on the surface, is estimated to be 200 ng/cm^2 . Only using diffusion according to Eq. 2.4 as a measure for the number of molecules attaching on the surface clearly gives an overestimate even for molecules with the highest affinity.

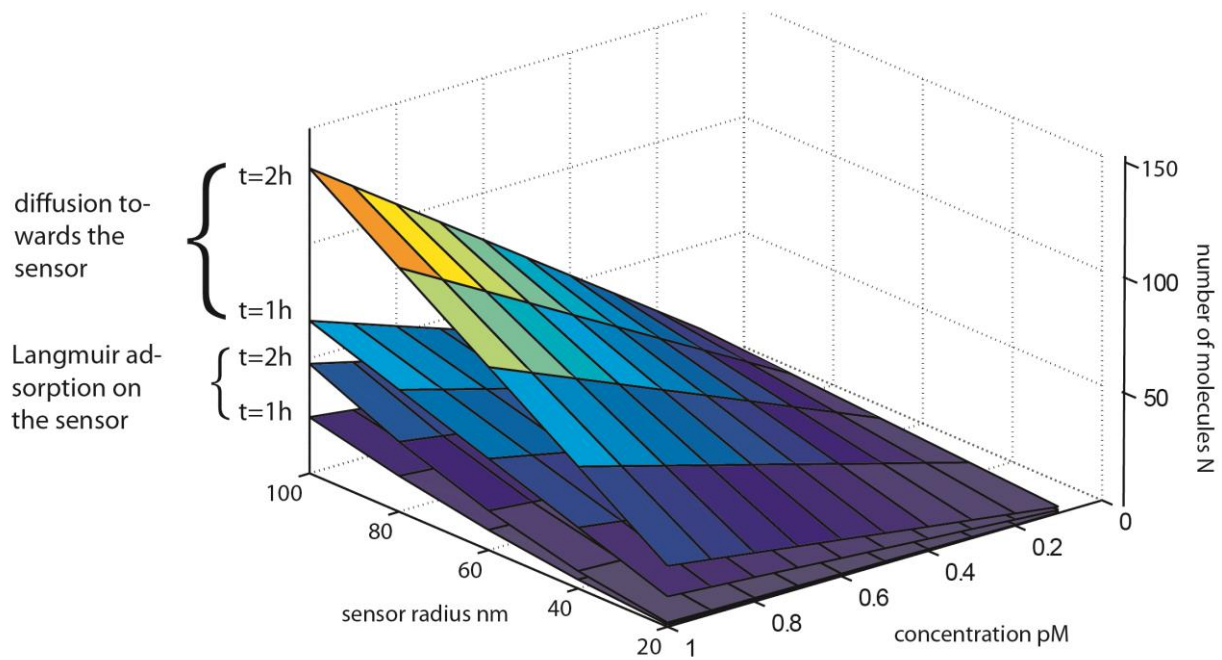


Figure 2-2. Number of molecules attached to the surface of a hemispherical sensor with varying diameter versus molecular concentration for one or two hours reaction duration.

When the diffusion of the analytes takes longer time to reach the surface than adsorption, the reaction is said to be mass transport limited. In order to determine in which of the two above mentioned rate limiting cases the system resides in, a dimensionless number, the Damköhler's number (Da), can be used.¹⁵ Damköhler's number is simply the ratio between the maximum reaction rate and the maximum diffusion rate. We can derive the Da number for our hemispherical model sensor from the linear term in the Langmuir isotherm Eq. (2.1) divided by the linear term in Eq. (2.4). The result is

$$Da = \frac{k_{on}\Gamma_{max}a}{D} . \quad (2.6)$$

Damköhler's number is simply the ratio between the reaction rate and the diffusion rate for a system. D is the diffusion coefficient for the diffusing molecule and a is the radius of the sensor surface. When $Da > 1$ the kinetic is mass transport limited and when $Da < 1$ the kinetics is reaction limited. The sensor design should always strive to minimize the Da number in order to speed up

the sensor response time. For a single hemisphere with a diameter of 100 nm and a Γ_{max} derived from above, $Da \approx 0.2$. For a macroscopic gold film with a reaction surface of 1 cm^2 , as in SPR biosensors, the Damköhler's number for streptavidin and biotin is $Da \approx 40000$. However, if the same experiment is performed on a nanostructured film with the same macroscopic dimensions but with gold nanostructures that only corresponds to 10% of the total gold film's area as in the experiments in paper **II**, the effective Γ_{max} is reduced correspondingly by a factor of ten. This also results in a ten times decrease in Damköhler's number. The higher number of molecules adsorbed on the nanostructured surface is therefore due to that the system is less diffusion limited.

To consider both the surface reaction and the diffusion limitation, the Langmuir isotherm (2.1) and Fick's second law of diffusion

$$\frac{\partial c}{\partial t} = D \frac{\partial^2 c}{\partial x^2}, \quad (2.7)$$

have to be coupled and solved together. Here x is the coordinate normal to the sensor surface. There is no analytical solution to this equation system. However, one can use finite element methods (FEM) to solve the equations for realistic cases, as illustrated in paper **III**.

In Figure 2-3, one such simulation is performed on a rod shaped particle with dimensions $60 \times 40 \times 120 \text{ nm}$ for different bulk concentrations. As comparison, the number of molecules from diffusion only and adsorption only calculated for a hemispherical sensor with same surface area are also shown. It is clear that when the sensor is reaction limited, the Langmuir isotherm describes the surface reaction fairly well.

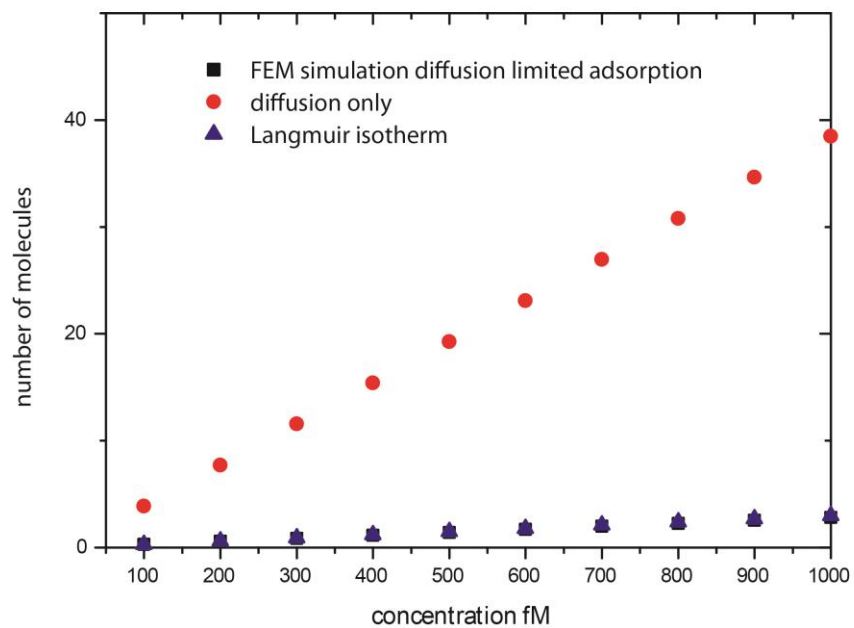


Figure 2-3. FEM simulation of the number of molecules that ends up on the nano sensor for diffusion limited adsorption compared to the cases of diffusion only and adsorption only.

Chapter 3 Introduction to plasmonic based refractive index sensors

Introduction to plasmonics

The interaction between a metal and visible light is mainly controlled by the free conduction electrons in the metal. The optical constants for gold and silver are shown in Figure 3-1. A quantized collective oscillation of the conduction electrons is called a plasmon. In certain special configurations the energy from light can be converted into plasmons. For instance, at metal dielectric interfaces, a propagating surface wave of oscillating electrons can be excited at optical frequencies. This surface charge density oscillation, with distinct resonance frequencies is called a surface plasmon resonance (SPR). Surface plasmon resonances are most pronounced in thin metal films and small metal particles. Nano sized gold and silver particles interact strongly with the incident light due to surface plasmons, giving rise to the bright colors of gold and silver colloids. This is also the reason behind many of the colorful medieval church windows, in which the glass was stained by colloidal particles.

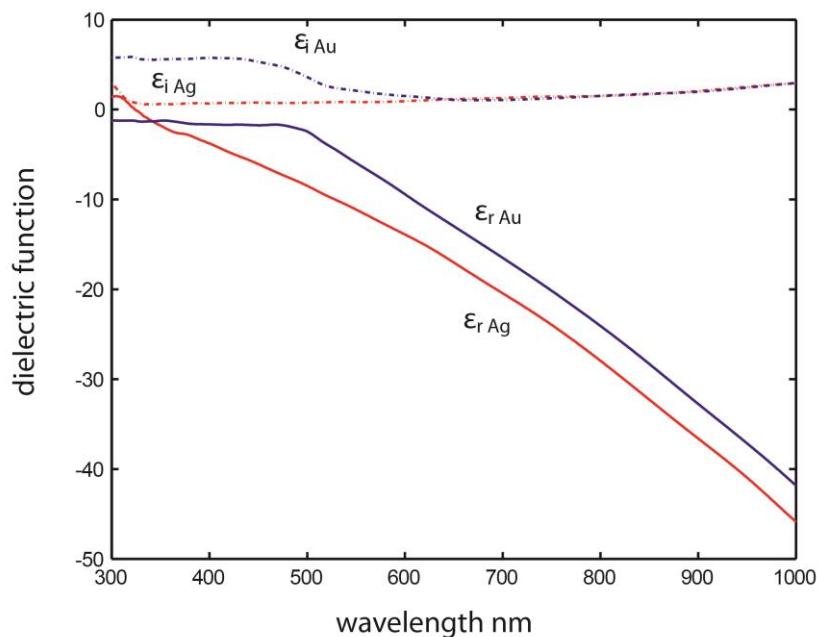


Figure 3-1. The experimental dielectric function of silver and gold, as reported by Johansson and Christy and Palik.^{16,17}

By solving Maxwell's equations for a metal dielectric interface, with proper boundary conditions, one finds an interface mode with wavenumber k_{spp} according to:¹⁸

$$k_{spp} = k_{ph} \sqrt{\frac{\epsilon_d \epsilon_m}{\epsilon_d + \epsilon_m}} \quad (3.1)$$

Here $k_{ph} = \frac{\omega}{c}$ is the wavenumber of the incident photon in vacuum parallel to the interface, while ϵ_d and ϵ_m are the dielectric functions for the dielectric medium and the metal, respectively. Noble metals such as silver and gold have a large negative real part of ϵ_m in the visible part of the electromagnetic spectrum, while the imaginary part of ϵ_m is small. At the interface between a metal film and a dielectric, k_{spp} has real component, which means that it is a propagating wave mode that runs along the interface. The damping of the propagating wave is given by the imaginary part of k_{spp} , which is due to the imaginary parts of the metal dielectric function and other losses. When the damping is small, the wave can propagate several mm along the surface of a thin film.

A propagating surface plasmon mode in a thin metal film, a so-called surface plasmon polariton (SPP), can only be excited in special configurations. As shown in Figure 3-2 (red line), the wave number of the photon is smaller than the wavenumber of the SPP mode. In order to excite the SPP, the momentum of the photon parallel to the surface has to match that of the SPP. By using a high refractive index prism to increase the momentum of the photon (green line), energy conservation and momentum conservation can be matched simultaneously. This so-called Kretschmann configuration is by far the most common method used to excite surface plasmons. From equation (3.1) it is clear that the wavenumber of the SPP mode depends on the dielectric medium through ϵ_m . By changing the dielectric, for example from air to water, the wavenumber of surface plasmon changes, which will in turn change the energy and the momentum needed to the excite the plasmon as illustrated in Figure 3-2.

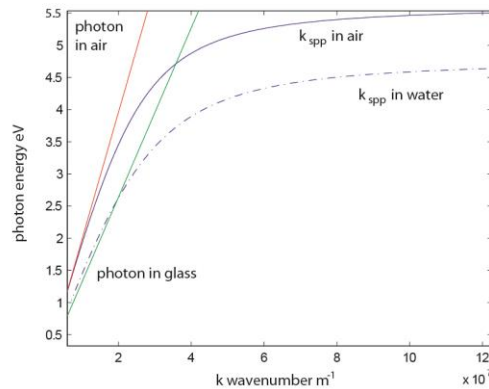


Figure 3-2. The dispersion relation of surface plasmons and light for an interface between a metal and a dielectric interface. The line show the photon energy versus wave number for light travelling parallel to the surface in air (red) and water (green) and the corresponding relation between the surface plasmon energy and wavenumber for an air-metal interface (blue) and a water-metal interface (dashed line).

Localised surface plasmon resonance

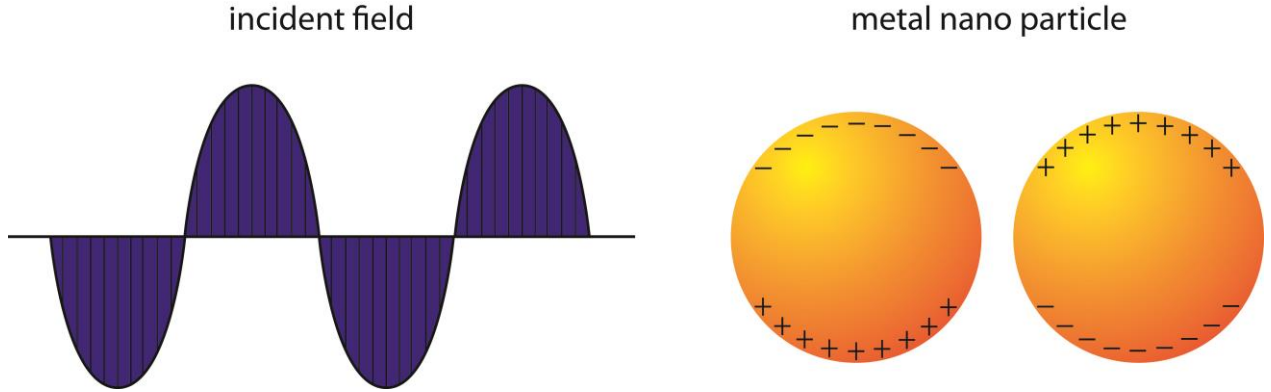


Figure 3-3. Schematic picture of nanoparticles interacting with light

The LSPR originate from resonance oscillations of the conduction electrons in the metallic particles induced by an incident electromagnetic wave. When a metal particle is much smaller than the wavelength of the incident light, the plasmon will not propagate as in the case of the thin film SPR. Instead, the field will force the electrons to oscillate within the particle's physical boundary under the influence of the external field. The positive ion lattice of the metal particle creates a restoring force due to Coulomb attraction similar to a spring in an harmonic oscillator, see Figure 3-3. In the so called quasi-static approximation, a small sphere with radius $a \ll \lambda$ is subject to an electric field $\mathbf{E}_0 = E_0 e^{-i\omega t}$. The induced dipole moment of the sphere is given by

$$\mathbf{P} = \varepsilon_0 \varepsilon_d \alpha \mathbf{E}_0 \quad (3.2)$$

with the polarizability function

$$\alpha = 4\pi a^3 \frac{\varepsilon_m - \varepsilon_d}{\varepsilon_m + 2\varepsilon_d}. \quad (3.3)$$

Here ε_m is the dielectric function of the metal ε_d is the dielectric constant of the environment, as before, and ε_0 is the vacuum permittivity. A resonance is obtained when $|\varepsilon_m + 2\varepsilon_d|$ is minimized, that is when $\varepsilon_m(\lambda) = -2\varepsilon_d$. The interaction between the incident light and the particles is then maximized.

The scattering cross section of the particle can be written as:

$$C_{sca} = \frac{8}{3} \pi a^6 k^4 \left| \frac{\varepsilon_m - \varepsilon_d}{\varepsilon_m + 2\varepsilon_d} \right|^2, \quad (3.4)$$

and the adsorption is

$$C_{ads} = 4\pi a^3 k \text{Im} \left\{ \frac{\epsilon_m - \epsilon_d}{\epsilon_m + 2\epsilon_d} \right\} \quad (3.5)$$

The experimental cross section is then given by the sum $C_{ext} = C_{sca} + C_{ads}$. From Eq. 3.4 and 3.5, the absorption cross-section is proportional to the particle's volume while the scattering cross section is proportional to its volume squared. When measuring the scattering intensity of a particle, in e.g. a dark field microscope, a larger particle thus gives more scattered photons compared to a smaller particle. When the particles get smaller, the scattering intensity drops like r^6 compared to absorption, which drops like r^3 . At around a radius of 10 – 15 nm, the signal-to-noise ratio starts to favor absorption measurements.¹⁹

If the nanoparticle is not a sphere, the polarizability function will be different from Eq. (3.3). It turns out that an elongated particle has an LSPR that is red shifted compared to a spherical particle. The reason behind this is that the restoring force from the positive lattice is reduced along the elongated axis and therefore, the resonance occurs at a lower frequency (longer wavelength). By simply changing the shape of a nanoparticle, one can thus tune the localized surface plasmon resonance to occur in the wavelength region of interest. Figure 3-4, shows substrates with gold nano-disks of the same thickness but different diameters. An increase in the aspect ratio with increasing disk diameters obviously moves the resonance position towards the red. Figure 3-4 also shown the effect of changing the dielectric around the nanodisk.

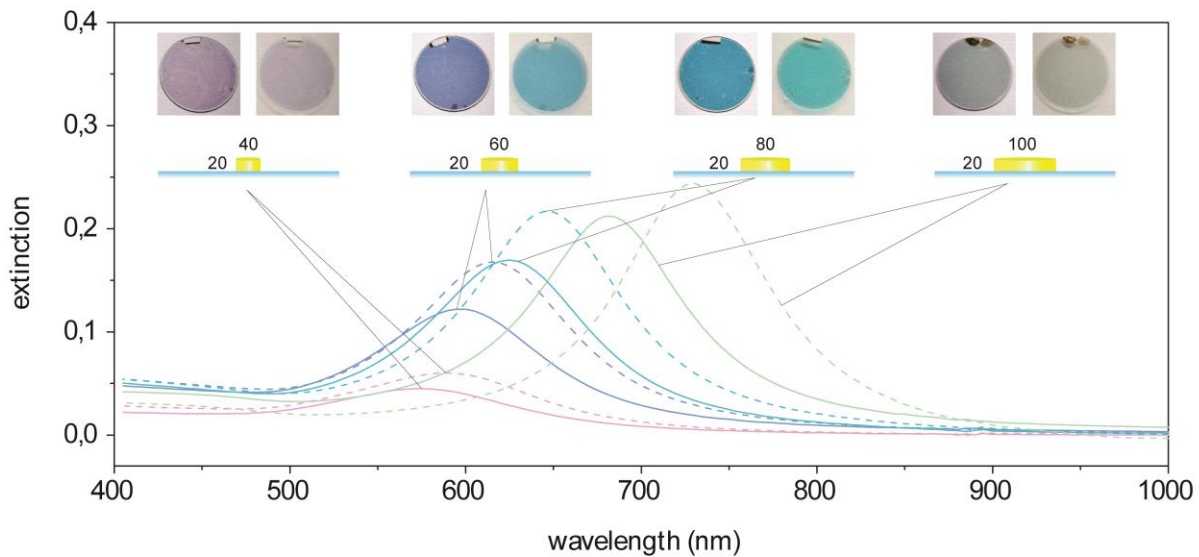


Figure 3-4. Nanodisk substrates with four different aspect ratios produced by hole-mask colloidal lithography. The samples were photographed in air (left samples) and in water (right samples). The particles are all 20 nm in height and the diameters are 40, 60, 80 or 100 nm. The corresponding extinction spectra in both air (solid line) and water (dash line) are also shown.

If a metal particle is moved from vacuum to a dielectric medium with a higher ϵ_d , e.g. water, the polarized electrons concentrated at the surface of the particle will polarize the dielectric medium in the immediate vicinity of the particle. This polarized dielectric will reduce the Coulomb attraction from the positive lattice of the metal particle, thereby decreasing the “spring constant” and the resonance frequency. The higher dielectric constant, the more the Coulomb force will be reduced.

The induced field from the oscillating electrons in the metal particle is extremely concentrated around the particle surface. The total field outside the nanoparticle is the sum of the incident field and the field induced by the nanoparticle, but at the LSP resonance, the induced field could be orders of magnitude larger than the incident field. However, it is also extremely distance dependent, since the intensity usually decreases as $1/r^3$. The extremely confined LSPR field is the origin behind many surface-enhanced optical phenomena, e.g. surface-enhanced Raman scattering and surface-enhanced fluorescence. Confined fields in gaps between particle dimers has been used to demonstrate single molecule detection by SERS,²⁰ refractive index sensing.²¹

Biosensing with plasmons

In a typical sensing experiment with LSPR, a biomolecule is bound to the surface of the plasmonic structures. The ambient dielectric is then changed from water to the biomolecules, which has a dielectric constant higher than the water. For a typical protein, the refractive index is about 1.46 compared to waters 1.33. The amount of adsorbed biomolecules can be traced by the LSPR peak position λ_{max} .

The refractive index sensitivity can be obtained by differentiating the resonance condition of λ_{LSPR} with respect to the refractive index of the medium n ,²²

$$\frac{\partial \lambda_{LSPR}}{\partial n} = 2\epsilon_m^r/n \frac{\partial \epsilon_m^r}{\partial \lambda}. \quad (3.6)$$

The sensitivity of the LSPR particle is proportional to the real part of the dielectric function of the metal ϵ_m^r and inversely proportional to the slope $\frac{\partial \epsilon_m^r}{\partial \lambda}$. Comparing the real parts of the dielectric functions of gold and silver, in Figure 3-2, the slope of the two is almost same. However, the absolute value of the real part of the dielectric function, ϵ_m^r , is larger for silver than for gold at all wavelengths. Together with an almost zero imaginary part of the dielectric function, this implies

that silver gives better plasmonic resonators and higher more sensitivity to refractive index changes. Despite this, gold is usually the metal of choice in sensor applications due to its chemical inertness compared to silver.

Selective adsorption of biomolecules to the surface can be done by first functionalizing with specific capture molecules, such as antibodies, antigens, nucleic acids or some other kinds of affinity based molecular system. The measured peak shift $\Delta\lambda$ can be used to estimate the effective refractive index change, Δn_{eff} , by

$$\Delta\lambda = S_{bulk}\Delta n_{eff}, \quad (3.7)$$

where S_{bulk} is the bulk refractive index sensitivity. The effective refractive index takes into account that the induced electromagnetic field only extends a small distance from the surface of the nanoparticles, thereby defining the sensing volume of the LSPR. The field can in the simplest case be approximated by an exponential decay, $E(z) = E_0\exp(-z/l_d)$ with a decay length l_d , where z is the distance from the particle surface. The sensitivity towards a refractive index change will therefore be reduced with increasing z . An effective refractive index can then be defined as

$$\Delta n_{eff} = \frac{2}{l_d} \int_0^{\infty} (n(z) - n_{medium}) \exp(-z/l_d)^2 dz, \quad (3.8)$$

where n_{medium} is the refractive index of the medium in which the experiment is performed, e.g. air, water or buffer.²³ S_{bulk} is the bulk refractive index sensitivity, expressed in peak shift per refractive index unit (nm/RIU). The bulk refractive index sensitivity is usually measured by monitoring the peak shift $\Delta\lambda$ while changing between media with different refractive indices, for example water with different glycerol concentrations. The most sensitive place is obviously at the surface of the nanoparticle. However the surface is often occupied by a layer of capturing agents such as antibodies. This means that the decay length needs to somehow be matched to the sensing experiment.

The field decay length l_d can be experimentally obtained by depositing of a dielectric while monitoring the LSPR peak position change. In Figure 3-5, nanostructures with two different dimensions i.e. 120 nm in diameter with 30 nm height and 100 nm in diameter with 70 nm height are compared and for deposition of alumina and silicon dioxide, respectively. The decay length of the field estimated this way was $l_d = 38$ nm for the high aspect ratio discs and $l_d = 28$ nm for the low aspect ratio disc.

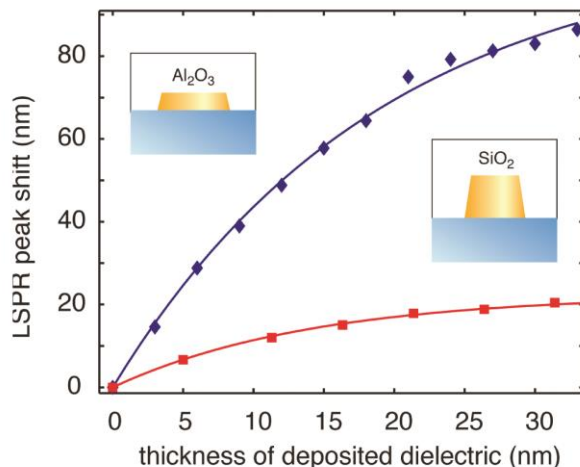


Figure 3-5. Measurement of the LSPR sensing range by deposition of dielectric material on the particle. A decay length of $l_d = 38$ nm for the high aspect ratio discs and $l_d = 28$ nm for the low aspect ratio disks are obtained by fitting to an exponential decay.

From the measured peak shift $\Delta\lambda$, the change of refractive index Δn could be calculated from equation (3.7). The calculated refractive index change can then be converted to the mass of the protein layer by de Feijter's formula.²⁴

$$\Gamma = \frac{d\Delta n_{eff}}{\partial n/\partial c} \quad (3.9)$$

where Γ is the surface mass and d is the protein thickness, $\partial n/\partial c$ is usually set to $0,182 / \text{cm}^3$ for proteins.²⁴ By utilizing the particles refractive index sensitivity, the decay length and the physical dimension of the bio molecules, the amount of adsorbed proteins on the surface of the nanoparticles can be estimated through Eq. (3.7), (3.8) and (3.9).

The peak shift induced by a single molecule adsorption event is very dependent on the optical mass of the molecule. Larger molecules occupy more of the induced plasmon field, which results in a larger peak shift. This strategy has been explored by labeling the analyte molecules with something with a larger optical mass, such as gold colloids or a larger protein.²⁵⁻²⁶ Average protein sizes are ~ 55 kDa, the size should be comparable with the dimension of streptavidin which is ~ 5 nm in diameter. In order to detect a single unlabeled protein, the field of the particle should match the size of the molecule.

I will estimate the peak shift induced by a single molecule using the fact that field decay length of a single hemispherical particle is approximately half the particle radius.²⁷ The hemisphere has no sharp corners and the field is evenly distributed with no “hot spots”. Therefore the peak shift for a single molecule of 2.5 nm in radius is:

$$\Delta\lambda_{single} = \frac{\Delta\lambda_{saturation}}{2\pi a^2/\pi r^2} \quad 3.10$$

where $\Delta\lambda_{saturation}$ is the peak shift from a full monolayer of the proteins with a thickness of 5 nm, $r = \frac{5}{2}$. In the denominator, $2\pi a^2$ is the surface area of the sensor and πr^2 is the foot print of the molecule. $\Delta\lambda_{saturation}$ can be expressed as:

$$\Delta\lambda_{saturation} = S_{bulk}\Delta n(1 - \exp(\frac{-4r}{a/2})) \quad 3.11$$

Taylor expansion on $(1 - \exp(\frac{-4r}{a/2}))$ results in $\frac{4r}{a} - \left(\frac{4r}{a}\right)^2 \dots$ where the square term and terms with higher power can be dropped since the sensor size is much larger than the molecule,. The resulting single molecule peak shift is then:

$$\Delta\lambda_{single} \approx \frac{4S_{bulk}\Delta nr^3}{a^3} \quad 3.12$$

In Figure 3-6 shows the estimated peak shift from one molecule with the average induced peak shift per protein for different particle size and different particle sensitivity is plotted with Eq. 3.10. Antosiewicz et al²⁸ has shown, using with the coupled dipole approximation, that the LSPR frequency shifts is given by:

$$\Delta\omega \sim -\frac{1}{2} \frac{V_1 n^2 - 1}{V_2 n^2 + 2}, \quad 3.13$$

where V_2 is the volume of the sensor and V_1 is the volume of the analyte molecule. The plasmon shift is thus indeed inversely proportional the sensor volume has also been concluded by other groups.²⁹

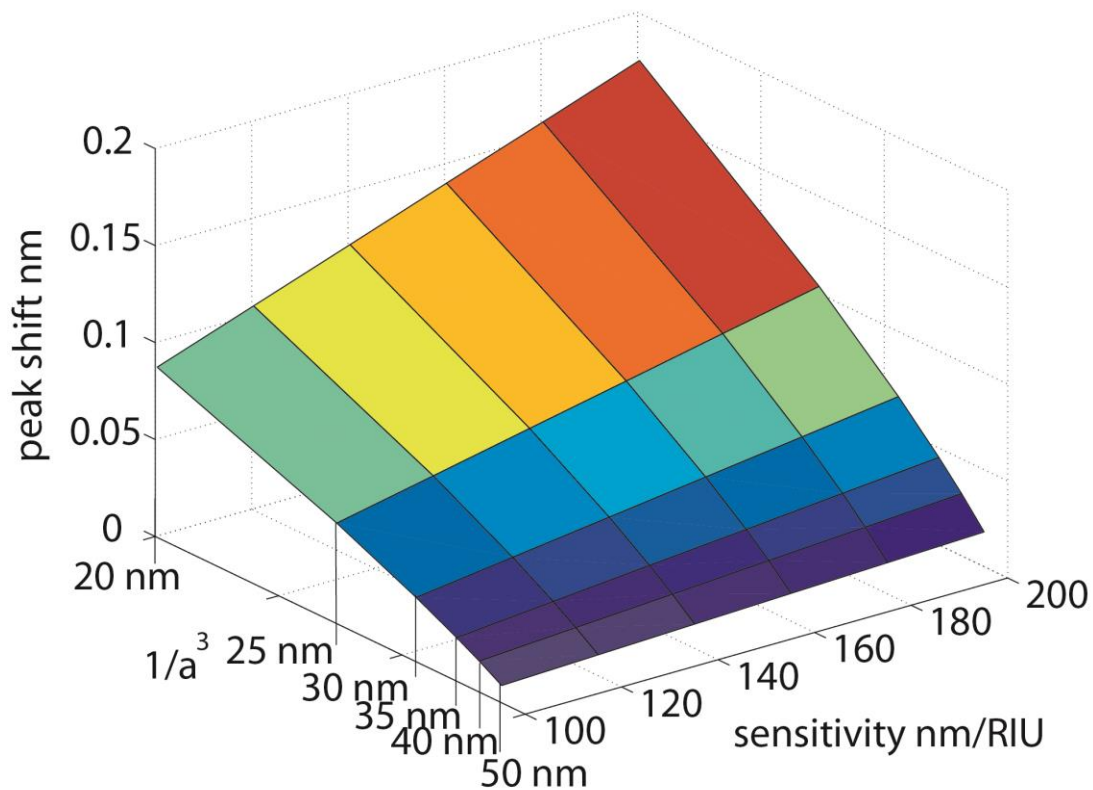


Figure 3-6. Peak shift induced by a single protein molecule with a radius of 2,5 nm adsorbing with radius a on a sensitivity between 100 and 200 nm per refractive index unit (RIU). The refractive index contrast Δn was 0.13.

Single molecule LSPR sensing has been reported for highly irregular nanoparticles,³⁰ but most previous studies have only been able to resolve full or close to full monolayer protein coverage.³¹⁻³² Only with recently advances in experimental methodologies, has it been possible to detect single unlabeled protein molecule adsorption using LSPR sensing.^{29, 33} The experiments were in both cases performed on very small particles.

Chapter 4 Fabrication of nanoparticles

One of the driving forces behind modern plasmonic research is the relatively recent ability to manufacture nanostructures with great versatility and precision. Nanostructures could either be fabricated in a top-down or a bottom-up fashion. Both fabrication principles have advantages and disadvantages. Among bottom-up nanofabrication techniques, the most frequently appearing type in the literature are different variations of colloidal lithography, such as nanosphere lithography for making hexagons of triangles,³⁴ or hole mask colloidal lithography (HCL).³⁵ In comparison with electron beam lithography, colloidal lithographic methods are cheaper and it is easier to produce large surfaces. Colloidal lithography, such as HCL described below, can produce homogenous substrates in cm^2 size with up to 40 % surface coverage. Producing a substrate like that requires at least a year with electron beam lithography (EBL). The HCL structures are short range ordered and relies only on the colloidal particle charge repulsion for self-assembly. Therefore the surface interparticle distance is relatively fixed. By introducing ions to screen the particle-particle charge repulsion, the interparticle distance can be slightly reduced. Substrates of this kind are mostly useful for large area extinction measurements. Since the self-assembled interparticle distance is much smaller than the optical diffraction limit, the only way to see individual particle is to increase the particle distance by diluting the particle concentration so much that the particle randomly adsorb on the surface. This approach can produce optically resolvable but randomly positioned single particles. The biggest disadvantage of HCL, or any other colloidal lithography technique, is the limited range of nanostructure shapes that can be produced. The shapes of the nanostructures are defined by the size and shape of the colloidal particle, which have spherical shape. However, playing with angled evaporations, angled etching, or using various shadow effects created by the mask, it is possible to produce ellipsoids, cones, crescent, rings, triangles and dimers etc.³⁵⁻³⁶

Hole mask colloidal lithography

The basic steps of hole mask lithography is shown in Figure 4-1. First a sacrificial layer of poly methyl methacrylate (PMMA) is spin coated on the surface of a piranha cleaned glass slide. Figure 4-1a. The substrate is then soft-baked for 10 minutes in the oven at 180 °C. The resulting layer of PMMA depends on the weight percent and the spin speed. The substrate is then oxygen etched for 5s (plasma batch top) to decrease the hydrophobicity of the PMMA surface and allow for wetting with water. Negatively charged poly-(diallyldimethylammonium) chloride (PDDA), is applied on the surface in order to attract the positively charged polystyrene particles (PS). The final size of the nanostructure is defined by the PS particles.

As shown in Figure 4-1 b-f, after the colloid particles have been adsorbed on the surface, a 10 nm layer of metal is evaporated on the PS covered surface to form a mask. The metal covered PS particles are then removed by tape stripping. The subsequent O_2 plasma etching will create holes

in the PMMA. The metal nanostructures are formed through metal deposition inside the hole. The HCL substrate is completed by dissolving the sacrificial layer in the final liftoff process, Figure 4-1b-f.

The O₂ plasma etching creates undercuts in the PMMA layers so that the liftoff step can remove the whole resist layer with ease. The undercut could be increased by increasing the O₂ etching time. If the undercuts is large enough, two angular evaporations can be performed. In the angular evaporation, two particles of the same or two different metals can be made with edge to edge separation below ten nanometers, see Figure 4-1g-h.

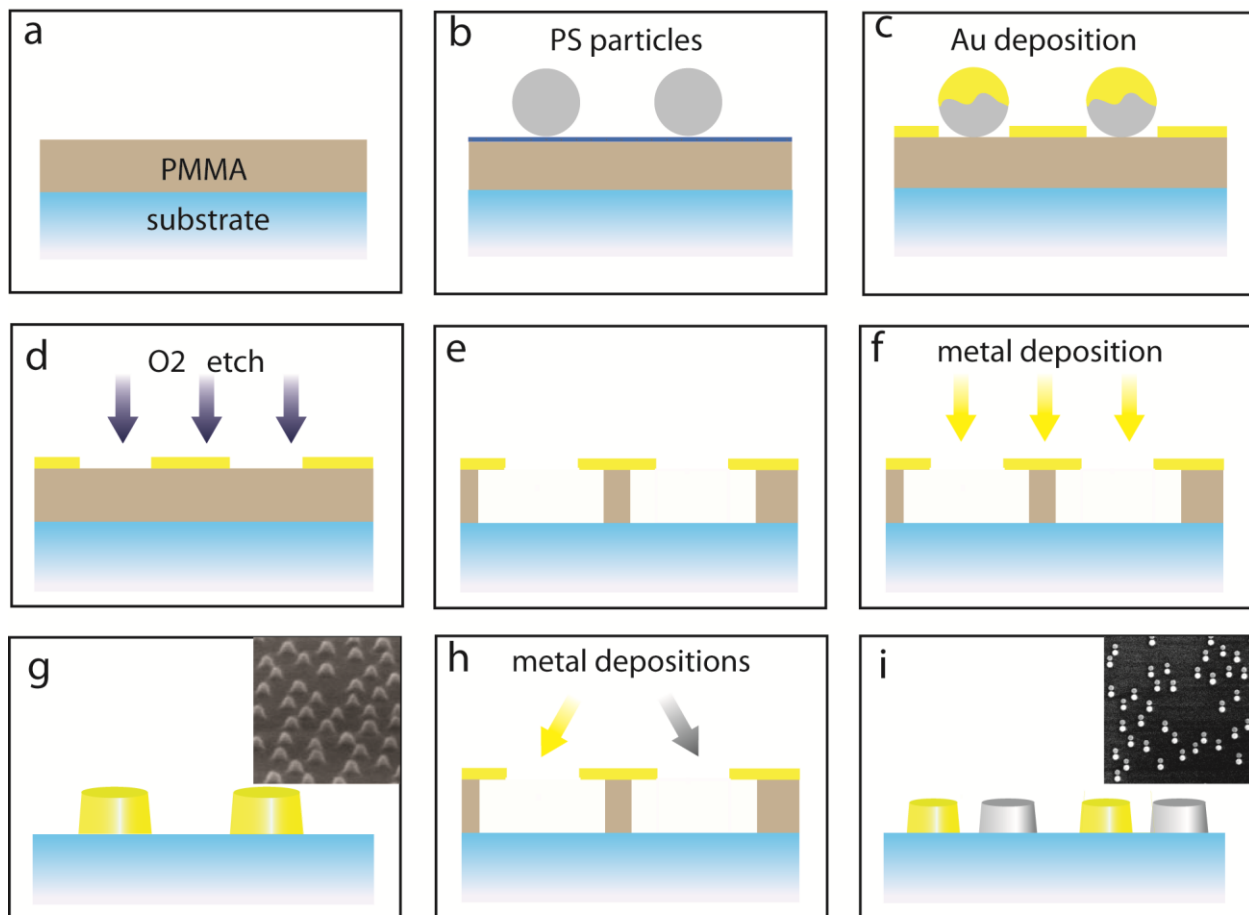


Figure 4-1. a-g)The steps involved in fabrication of HCL samples. h-i) variations of HCL may produce dimers with different metals. inset g) Sideview of gold nanoparticles produced by HCL. inset i) dimers of gold and silver with gap size ~10 nm.

Electron beam lithography

Electron beam lithography (EBL),³⁷ focused ion beam etching (FIB) and nano imprinting³⁸ are some of the most used top down nanofabrication techniques. The main strength of the top down techniques is that the user has control of the design and the placement of the nanostructures. However, top down techniques, such as EBL, is time-consuming and expensive, in particular for any larger surface coverage, and therefore nanoplasmonic EBL structures are mostly used in various optical microscopy studies.

The principle of EBL is straightforward; a thin layer of e-beam resist is spin coated on a substrate and structures in the resist are written by an electron beam. The machine is similar to an ordinary electron microscope with electrons accelerated from the emitter and de-magnified on the surface. The e-beam resists used are electron sensitive polymers that either crosslink or break when exposed to the e-beam. If a positive resist is used, the exposed parts are dissolved in the development phase. The pattern is transferred from the resist to the final metal structures in a similar fashion as in HCL, i.e. the metal is first deposited on the structures before removal of the resist in the lift off.

Unlike the photolithographic methods, where the resolution is limited by the wavelength of the exposure to UV light, the de Broglie wavelength of accelerated electrons is very short. It is typically 0,01 nm for an acceleration voltage of 50 kV. In reality the beam size is around a few nanometers in diameter. However, the limiting factor is not the beam size but the backscattered electrons. Backscattered electrons are electrons that scatter back from the substrate into the resist layer, thereby exposing the resist a second time. This so-called proximity effect reduces the resolution and cause pattern variations. The proximity effect can be reduced by using a double layer resist with a thin structure-defining layer on top, so that the dose requirement can be reduced and the second layer of resist can filter away part of the secondary electrons.

Using a double layer resist also results in more successful lift off processes. An undercut can be created in EBL in the lower resist layer. The layer in the bottom has a higher sensitivity towards electrons compared to the layer on top, so that the bottom layer is more exposed compared to the top layer. After two developments of the structure, first of the top layer and then of the bottom layer, a natural undercut is created. Another benefit from using the double layer is that structures with larger aspect ratio can be created compared to a single layer structure.

Figure 4-2a-e shows the important steps in the EBL fabrication that has been used in my studies. A double resist layer consisting of methyl methacrylate (MMA) as the low molecular weight resist and ZEP as the high molecular weight resist. On top of the top resist layer, a metal film by gold or chromium is required in order to remove the charges from the electron beam during the exposure. After the electron beam exposure, the low molecular weight layer of MMA is over exposed compared to the high molecular weight layer ZEP, as shown in Figure 4-2b. The metal layer is first etched before the two resists are dissolved in developers. Gold is evaporated through the ZEP layer to form the final metal structure, Figure 4-2 d. Due to the over exposure of the lower layer of the resist, the lift off process is very easy to perform.

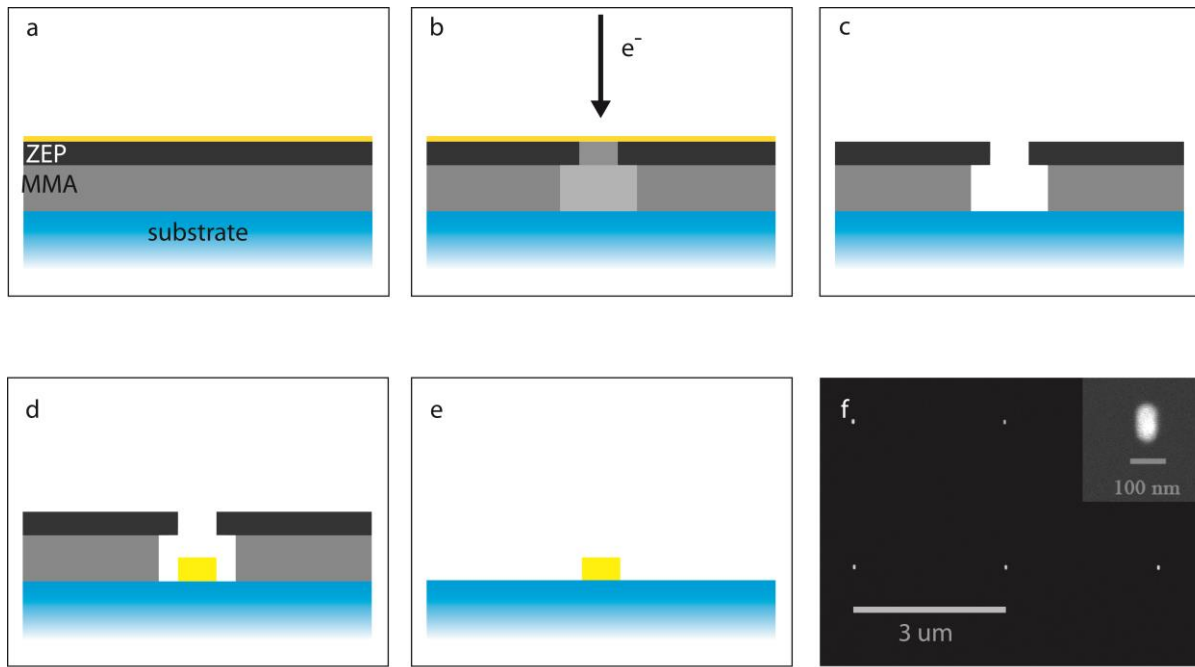


Figure 4-2. a-e) The steps involved in fabrication of EBL samples. f) SEM image of single particle array produced by EBL. inset f) magnified SEM image of a single nano rod made by EBL.

Chapter 5 Schemes of measurement and analysis

Optical measurements

The first things one note with noble metal nanoparticles are the different colors they display. Extinction measurements are the most straightforward way to quantify the colors, i.e. the optical response of the nanoparticles. Figure 5-1 illustrates experimental schemes for extinction and scattering measurement of LSPR substrates. Extinction measurement measures the loss of light passing through the sample and is defined as.

$$Ext(\lambda) = \log \frac{I_0(\lambda)}{I_t(\lambda)}, \quad (5.1)$$

where I_0 and I_t are the incoming light and transmitted light. Extinction spectroscopy is one of the most commonly used methods to study LSPR and to measure the peak shift induced by refractive index changes around nanoparticles. Since the nanoparticles can be excited from virtually any angle, no special configurations are required. The experimental requirements are small: a halogen lamp as light source and a simple spectrometer are all that is needed. In the case of dense particle layers, when the LSPR surface behave more like a homogenous surface, it is often more useful to talk about transmission and reflection rather than extinction and scattering.

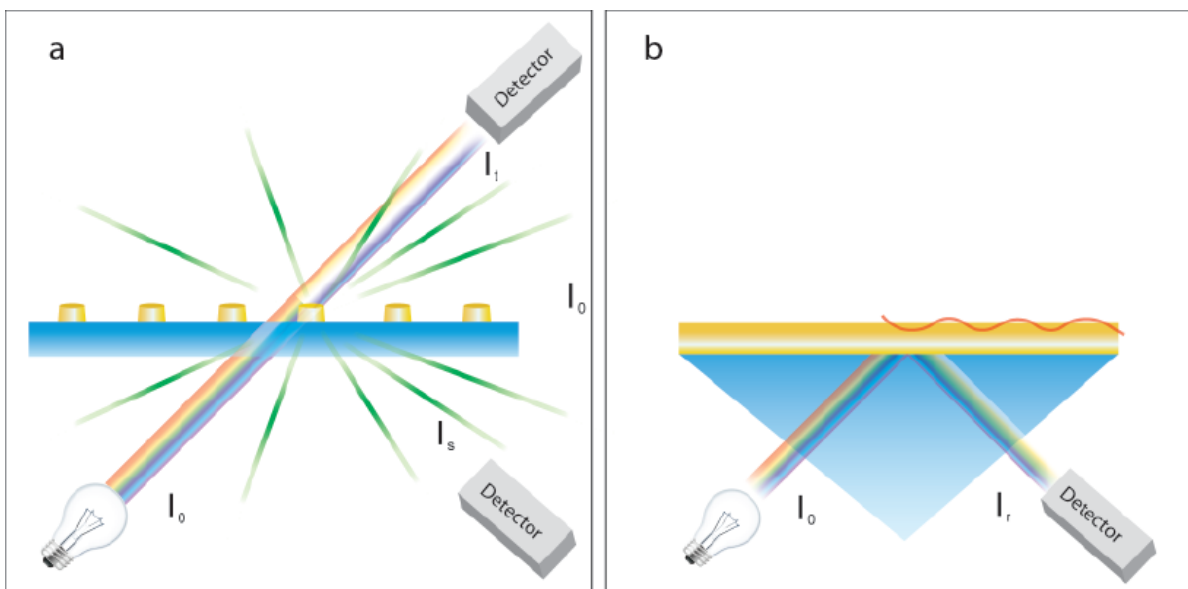


Figure 5-1. a) Extinction and scattering measurement of LSPR substrate. b) Kretschmann configuration of SPR measurement using white light.

In order to collect scattering from a particle layer using the same equipment, the scattering from the particles is simply collected from an angle separate from the directly transmitted light. The spectrum of scattered light I_s has to be normalized to the incident light spectrum I_0 in order to get the real scattering spectrum:

$$Sca(\lambda) \propto \frac{I_s(\lambda)}{I_0(\lambda)} . \quad (5.2)$$

In a typical thin film SPR measurement in the Kretschmann configuration, see Figure 5-1b, the light source is either a single wavelength laser or a white light source. In the first case, the light is focused on the metal film, thereby giving multiple incident angles in an attenuated total internal reflection mode. Since only a certain angle contains the correct k_x component for SPR, the light will be absorbed for a specific reflection angle that can be resolved by a CCD array. When using a white light source, the light is instead collimated so that photons with correct energy are used to excite the SPR. For a given incidence angle, the reflected spectrum then shows a dip at λ_{SPR} .

Micro extinction and dark field measurements

Extinction measurements can be performed in a microscope with the probed area orders of magnitude reduced compared to spectrometer measurement without compromising the accuracy of the peak position measurements. When measuring extinction in a microscope, the objective should have a low numeric aperture (NA) in order to reduce the amount of scattered light gathered by the spectrometer. However if the density of particles on the substrate is very low, as in single particle experiments, dark field (DF) scattering measurements is more favorable compared to extinction measurements.

In order to perform a dark field (DF) measurement, a hollow cone of light illuminates the surface at an angle higher than the collection angle of the objective. In this way only the scattered light is collected. Objectives with high numeric aperture (NA) is desired for more efficient photon collection, but their NA has to be smaller than that of the DF condenser. For an air DF condenser, the maximum possible objective NA is $\sim 0,9$.

As previously discussed, LSPR sensors can be made small since they are not limited by the propagation length of the plasmon. The smallest possible LSPR sensor is obviously a simple nanoparticle. Dark field measurements on single particles can be done in several different ways. The simplest way to collect the scattered light from the particle is with a thin fiber placed directly at the position of the particle in the image plan of the microscope. The light collected from the

fiber is coupled to the spectrometer, which is usually equipped with a 1 D CCD array.³⁹ That spectrum measured from only one particle is collected by the small opening of the fiber.

The image from the particles on the sample stage can also be imaged at the slit of the spectrometer.⁴⁰ By closing the slit so that only one line of particles visible, the light from isolated particles can be spread on to individual lines of a 2D CCD camera. In this way, spectra from several individual particles can be measured at the same time. Methods that are based on limiting the number of particles highly limit the throughput of the experiments. In order to use single LSPR particles as individual sensors to study the stochastic biological process or sub-populations in a sample that would otherwise be obscured in an ensemble measurement, statistical analysis of large sample numbers is required. This is difficult to achieve with ordinary spectroscopy.

To study a statistically significant number of single particles with high throughput, imaging techniques has been utilized. Imaging particle arrays using a single wavelength is based on the intensity change induced by a peak shift. The power of this technique is the fast time resolution of the measurement. However, a drawback is that the measurement is very sensitive to other types of changes, such as vibrational changes if only one intensity is monitored. Since the spectral fluctuations in the form of peak position shift is horizontal to the changes in the intensity variations due to several types of noise, such as shot noise, read out noise and vibrational noise, obtaining the spectral information should in principal give better noise reduction than purely intensity based measurements. Using a tunable filter to image particles at different wavelengths to build up a 3D cube of images, with the third dimension being the spectral information, has been investigated by several groups. The maximum number of particles that can be studied is in principle only limited by the detector size and the diffraction limitation of the light.⁴¹⁻⁴² However, the high throughput and accuracy in spectral information also result in poor time resolution. Recent advantages in single particle imaging has resulted in several other innovative techniques, such as objective grating imaging.⁴³

Single particle spectral imaging and image analysis

Even though an image says more than thousand words, a spectrum gives much more detailed information than merely intensity readings. The use of tunable filters for spatial and spectral imaging can be found in many applications in various fields of science and technology where both spectral and spatial information are required, from observing the biggest know objects such as stars, the Earth and environment monitoring, to the smallest observable things such as nanoparticles.⁴⁴⁻⁴⁶

Two most general methods for the wavelength selection are to either spread the beam of light into its full spectrum based on diffraction and refraction or to transmit only specific wavelengths using band-pass filters. Although diffraction gratings offer superior spectral resolution and easier

wavelength readings, they are difficult to use for two dimensional spatial imaging. Filters, on the other, hand offers better spatial imaging solutions but lack the spectral resolution that is offered by the diffraction gratings.

The liquid crystal tunable filter (LCTF) used throughout this thesis is based on the classical Lyot-Öhman design. It is based on two linear polarizers with a birefringent material in the middle. Depending on the vacuum wavelength of the light λ_0 and the thickness of the birefringent material L , the phase Γ will be:

$$\Gamma = \frac{2\pi\Delta nL}{\lambda_0} \quad 5.3$$

where the Δn is the difference in refractive index between the two polarization in the birefringent material. The transmitted intensity T in a single cell is

$$T = \cos^2(\Gamma/2) \quad 5.4$$

The transmitted light from the multiples of Γ beside the central wavelength need to be suppressed by multiple cells with retarder length increased with a factor of 2 for each cell, so that the transmission minima overlaps with the transmission maxima, which can be seen in the transmission profile of each individual cell with different L in Figure 5.2, where the last images shows the transmission profile through all of four cells.

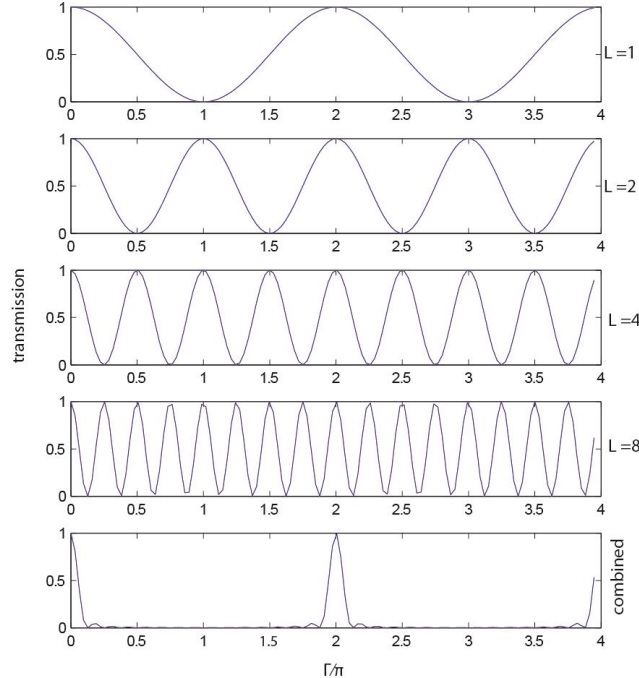


Figure 5-2. The transmission profile through Lyot Öhman filter with four different cell lengths and the combined transmission for four cells together.⁴⁵

The drawback of this kind of filter is that it cannot have high spectral resolution without being extremely thick, due to the requirement of multiple cells. This is also the reason why LCTF filters are usually bulky and cannot be placed in front of the cameras without additional lens systems. In addition to the retarder, a liquid crystal layer is added. The liquid crystal molecules are dipolar and birefringent molecules that upon an applied potential reorient its axis which consequently changes its retardation. The retardation of the liquid crystals can be changed continuously by the applied potential, consequently changing the transmission wavelength continuously.

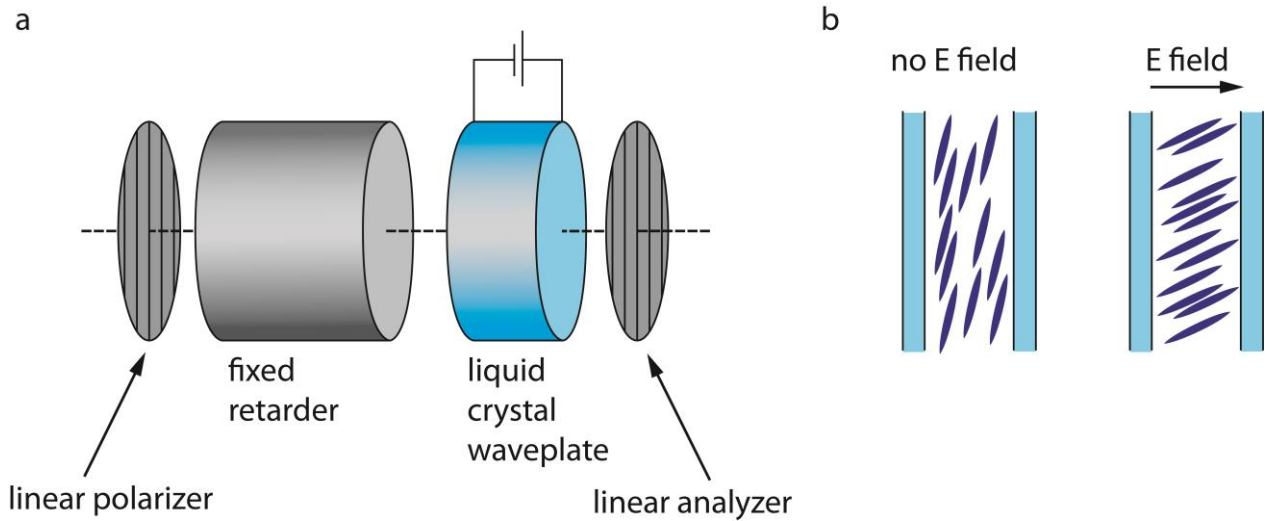


Figure 5-3. a) A single cell in LCTF. A single cell in LCTF consists of two linear polarizer and a fixed retarder and a liquid crystal retarder. b) The liquid crystal changes its orientation upon applied potential which tune the total retardation of the cell, consequently changes the transmission wavelength continuously.

In our measurements we have placed a liquid crystal tunable filter (LCTF) light path either in front of the lamp or in front of the camera. A LCTF selects a narrow part of the light spectrum with a typical bandwidth of 7 to 10 nm. By scanning through the whole spectrum with the LCTF while taking intensity images of all the particles in the field of view, a scattering intensity profile can be built for each of the particles. Hundreds of scattering spectra from individual particles could be obtained in one scan, see Figure 5-4. However the intensity at each wavelength needs to be collected in at least 1 second in order to get enough photons. One scan takes in general a few minutes for a single scan with 200 data points per spectrum. However faster kinetics can be achieved by reducing the number of data points.

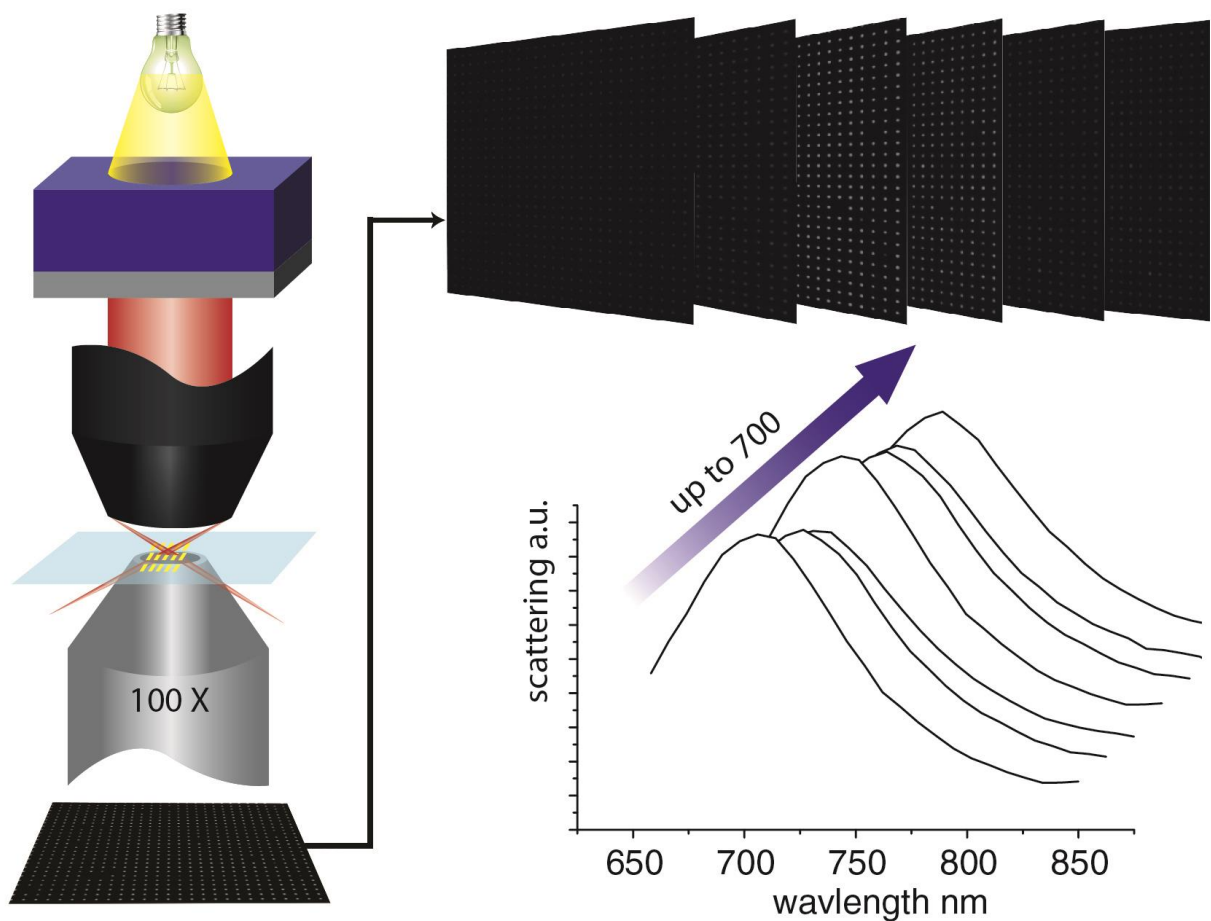


Figure 5-4. The white light from the lamp is first filtered by the LCTF before entering the dark field condenser. The scattered light collected by the objective is imaged by a 2D CCD camera. From the intensity images of the particles, up to 700 scattering spectra from individual particles can be constructed.

For single particle measurement, the substrate can be produced by both HCL and EBL. However, the inter-particle distances in HCL are not well controlled and it can be often difficult to separate two particles from each other if the distance between them is close to the diffraction limit. EBL is then a better choice to produce single particle sensor substrates because the particle distances and sizes can be well controlled. Figure 5-5 shows the scattering peak position distribution of up to 700 nanoparticles measured with LCTF in one single scan. The differences in peak positions of the nanoparticles are due to the inhomogeneity of the particles.

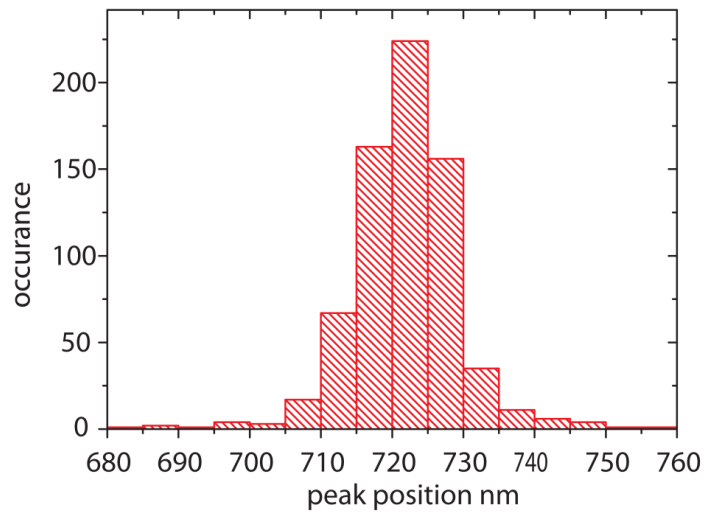


Figure 5-5. Nanorods prepared by EBL measured using the LCTF. The number of measured particles were 698.

One of the most important parts of the LCTF measurement is the image analysis. Figure 5-6 shows the intensity profile of a few nanoparticles on one line of pixels on the camera at 650 nm wavelength. The mass centers of the intensities for each of the particles are first extracted. Around each of the centroids, an octagonal mask is then drawn, defining the regions of interest. The number of pixels that is included in the analysis for a single particle is 74, which includes ~ 80 percent of the total counts corresponding to a single particle. The motivation of using a small number of pixels is to decrease the possible read out noise that is associated with the number of pixels.

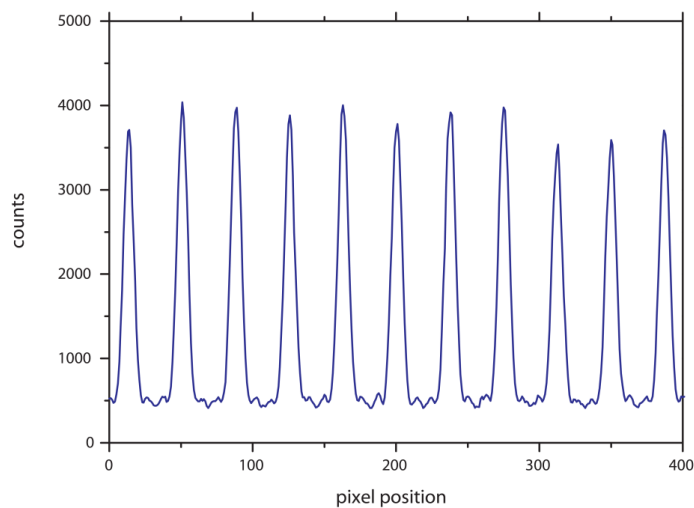


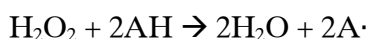
Figure 5-6. Intensity profile along one line of the pixels on the CCD camera.

The lamp spectrum is also collected in the same way as the particles, but with the objective aperture opened up instead. It is very essential to use the lamp spectrum from exact same pixels that are extracted for each of the particles due to inhomogeneous illumination and possible differences in the pixels response. The dark counts are measured with the shutter of the camera closed.

Chapter 6 Surface chemistry and biomolecules

HRP enzymology

Enzymes are one of the most usable classes of molecules in our body. Without their function, important chemical reactions cannot occur with sufficient rate for us to survive. Enzymes that are associated with hydroperoxides are among the most efficient enzymes known. Horseradish peroxidase (HRP) where the name is used very generically for the enzymes extracted from the root of horseradish, are in fact 15 different isoenzymes where HRP C is the most abundant one.⁴⁷ Its general reaction formula is



where AH and A· is the enzyme's reducing substrate and the resulting radical product. This may indicate that the possible *in vivo* functions in plants are cross-linking of cellular molecules through radical polymerization.⁴⁷ It was also found that certain isoenzymes of HRP are associated with wound healing of the plants.⁴⁸ The typical reducing substrates are aromatic phenols, phenolic acids, indoles and amines. The modern use of HRP in bioscience is mainly associated with the enzyme linked immuno sandwich assay (ELISA). Since its development in the 70s, which replaced the use of radio activity labeling, the technique have become the standard in many medical diagnostic assays.⁴⁹ In many assays, colorless and non-fluorescent molecules were made into substrate molecules for HRP. After reaction with HRP, the molecules are turned into marker molecules with color or fluorescence. The traditional ELISA assays are performed in 96 wellplates and readout by plate readers either by transmission or fluorescence measurement.

HRP have also been used for studying ultra-structures in cells with electron microscopy by precipitating a monomeric molecules into an electron dense polymer.⁵⁰ The precipitates are localized and forms only at the site of the HRP enzyme. The polymerization ability of HRP has also been investigated in aquatic phenol removal by polymerizing the toxic monomeric phenol into insoluble polyphenol which then can be removed.⁵¹ The most commonly used substrate for local precipitation with HRP for ultra-structure imaging in cells is 3,3'-diaminobezidine (DAB).

Figure 6-1 shows a simplified version of the full reaction cycle extracted for a fungal peroxidase.⁵² It can be assumed that the overall reaction cycle is valid for HRP as well. The native enzyme bound with two water molecules is replaced by a hydroperoxide molecule in the reaction center, which consists of a ferric heme structure (shown as the red square). The hydroperoxide first oxidize the reaction center of the enzyme by removing two electrons. One of the electrons comes from the metal core (Fe(III) → Fe(IV)), the other one results in a cation radical on the heme structure (compound I). Compound I is subsequently reduced twice by two hydrogen donators A-H to recreate the native enzyme. In the same process two radicals A· are produced, which can be used in a radical induced polymerization reaction.

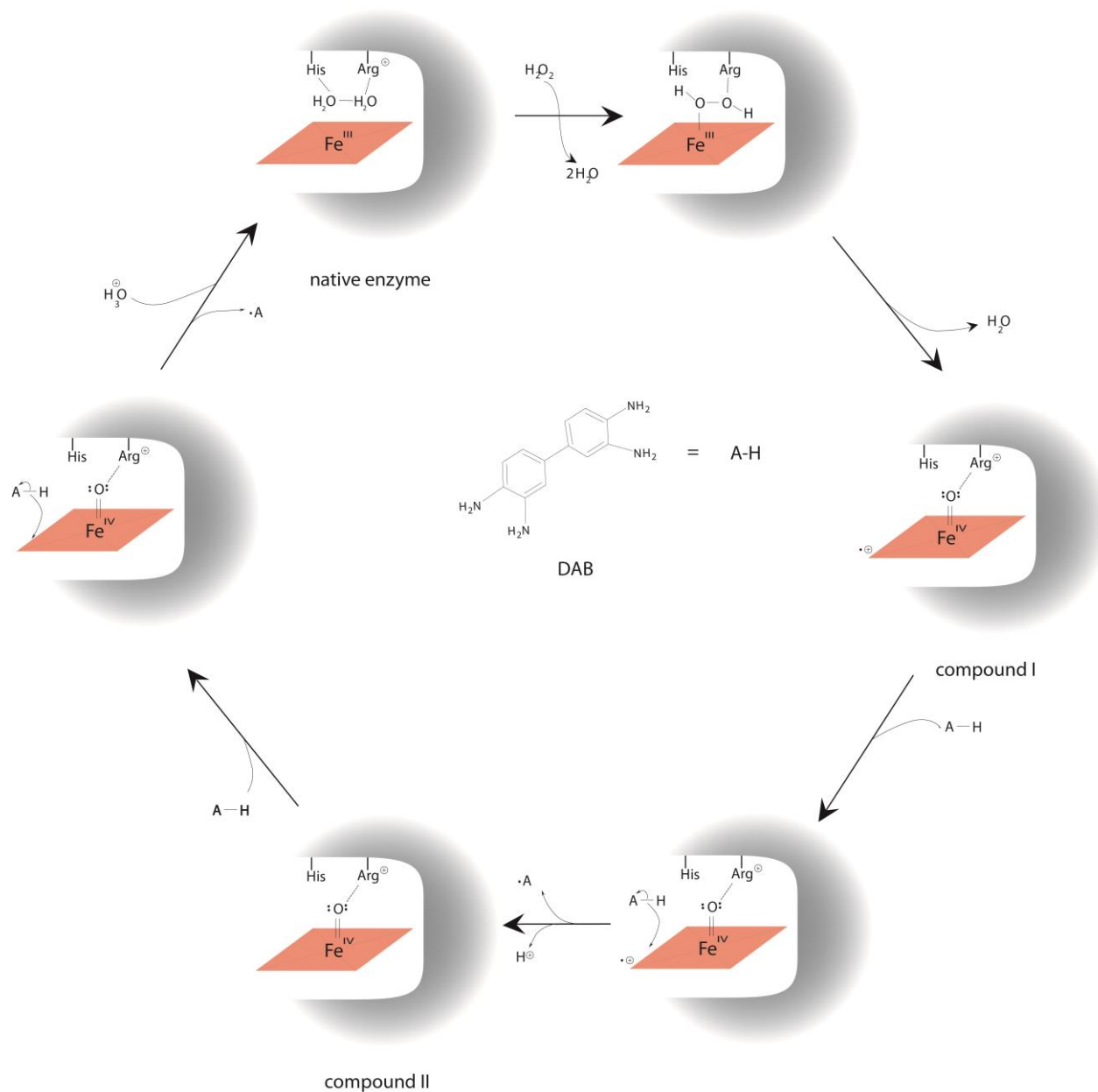


Figure 6-1. The catalytic reaction circle of a peroxidase. The native enzyme is first oxidised by peroxide to create compound I. The enzyme then goes through two reductions to create two A· radicals. Diaminobenzidine (DAB), shown in the middle of the figure, is one of the most popular HRP substrate.

New developments of techniques that are based on a combination of surface sensitive tools, such as SPR and LSPR, with enzymatic amplification, like ELISA, have been shown to be very powerful. The precipitated molecules by HRP on the surface can enhance the responses two orders of magnitudes for SPR and one order of magnitudes in LSPR.⁵³ The reason for the lower enhancement for LSPR is the shorter decay length of the electromagnetic field compared to the

propagating plasmon. However, we have shown that if the surface coverage of HRP is low, two orders of magnitudes enhancement is still obtainable.

Other groups have also been working on the concept of combining enzymatic amplification with plasmonic sensors. Most noticeably is the recent work done by Rodriguez-Lorenzo *et al*, where instead of using surface bound particles one used suspended colloidal particles for sensing. The claimed sensitivity was 10^{-20} M for an antibody antigen pair.¹³ If this holds true, this can be a very interesting sensor for the future ultrasensitive diagnostics since suspended particles certainly speaks for cost efficiency and read-out simplicity.

However, several considerations need to be addressed using enzymes for signal enhancement, especially in single molecule sensors. At the single molecule level, the seemingly identical copies of the enzymes show both heterogeneity of stationary properties so-called statistic disorder and the time-dependent fluctuations so-called dynamic disorder.⁵⁴ Using single molecule techniques to study single enzymes has resulted in new information that could not be obtained in ensemble measurements.⁵⁵ In single molecule sensors, the heterogeneity of the individual enzymes works to our disfavor. The major differences in responses due to the heterogeneity of the individual enzymes makes correct quantification difficult.

Self-assembled monolayers

Self-assembled monolayers (SAM) on different kinds of surfaces have been the key building block for many applications in nanotechnology. Especially in biosensor application, SAM's function as the linker that bridges the biochemical moieties with the solid state transducer. A typical SAM molecule includes three different parts with different functionalities. The head of the molecule anchor the molecule to the surface, the backbones of the molecules utilize the van der Waals interaction to stabilize the monolayer structure and the terminal group, which is the exposed part of the monolayer, adds the additional functions to the modified surface. Different SAM molecules have been developed for many different surfaces, e.g. silane based head groups forms SAM on silicon surfaces, alkanolic acids forms SAM on metal oxides and thiol based head groups forms SAM on gold surfaces.^{56,57}

Different terminal groups have also been developed depending on the requirement of the application. For examples, poly-ethylene-glycol moieties serve as a hydrophilic and human body friendly coverage for the colloidal surface and substrate; carboxylic acids can be utilized in amine coupling based chemistry to further modify the surface, and biotins provide surface binding sites for avidin molecules.

Streptavidin and biotin

Streptavidin is a tetrameric molecule with four binding pockets for biotin. Its molecular weight is 55 kDa. The dimension of the streptavidin molecule is 5,4x5,8x4,8 nm.⁵⁸ One of the strongest

known molecular interactions is between biotin and streptavidin. Here K_D is exceptionally low, approximately $10^{-15} \text{ M}^{-1}\text{s}^{-1}$ measured in solution.⁵⁹ Due to its strong interactions, it is one of the most often used bio-recognition pairs.

When molecules are bound to a surface, the binding constant may drastically decrease. Even though the affinity coefficients k_{on} and k_{off} for avidin and biotin are among the most measured properties, the literature values show a huge spread due to different experimental setups, conditions and different biotin surface concentrations. In table Table 6-1, I have summarized a few different biotin streptavidin binding constants and the special experimental conditions specified in the articles. The measured affinity constants vary within such a broad range that special considerations should be taken when comparing the results. A strong affinity coefficient between a monoclonal antibody and an antigen for PSA is also presented as a comparison.

$k_{\text{on}} \text{ M}^{-1}\text{s}^{-1}$	$k_{\text{off}} \text{ s}^{-1}$	K_D	Measurement
1.2×10^5	6×10^{-6}	$5 \times 10^{-11*}$	Fluorescent avidin binding to biotinylated lipid ⁶⁰
9×10^6	$7,2 \times 10^{-2}$	$8 \times 10^{-9*}$	SPR measurement ⁶¹
NA	$1,4 \times 10^{-5}$	NA	Biotinylated gold surface measured with SPR ⁶²
$4,7 \times 10^6$	NA	NA	Beads with bound SA binding to a surface ⁶³
$3 \times 10^6 - 4,5 \times 10^7$	NA	NA	Solution measurement using FRET ⁶⁴
NA	NA	10^{-11}	LSPR particles ⁶⁵
$5.3 \times 10^7*$	$0,9 \times 10^{-7}$	$1,6 \times 10^{-15}$	Measured in solution ⁵⁹
4×10^4	4×10^{-5}	1×10^{-9}	PSA-anti-PSA by SPR ⁶⁶

Table 6-1. Literature values for the biotin-avidin affinity constant show a wide spread of k_{on} and k_{off} values. *number calculated from the given literature values. For comparison a strong monoclonal antibody and antigen interaction for PSA is also given.

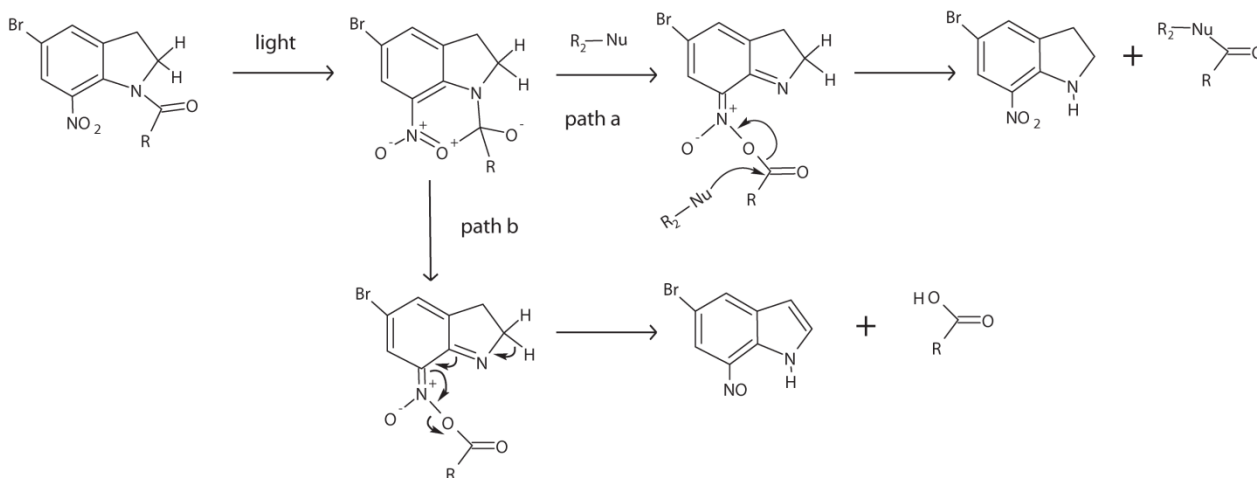
For surface based sensors the maximum number of binding sites for a molecule, Γ_{max} , is an important parameter to determine. Several studies have been performed by other groups to measure the saturated surface layer of streptavidin on a self-assembled monolayer with biotin. The obtained saturated streptavidin layer varies from 420 ng/cm^2 measured using QCM-D to 200 ng/cm^2 measured with SPR.^{58,62} If the saturated surface concentration is 420 nm/cm^2 , then each of the streptavidin molecules would only occupy an area of 22 nm^2 , less than the close packed form of streptavidin. However a closer look at the measurement techniques shows that QCM-D measures both the protein's mass and the water molecules trapped inside the protein layer. The hydration fraction is 58% measured by Nilebäck et al.⁶⁷ The mass measured by SPR is therefore more accurate. 200 ng/cm^2 gives a surface coverage of 60% of the total surface which is in very good

agreement with the maximum surface coverage one would expect from random sequential adsorption which is 55%.⁶⁸

Photochemistry and photofunctionalization

Using photons to activate specific parts of molecules to make specific reactions possible is very interesting for both biochemistry and organic synthesis, because it is a rather clean process without additional activator chemicals. Special efforts have been made to synthesize functional molecules that can be activated by visible or blue light, in order to avoid deep UV light that may destroy other molecules that are not participating in the reaction. One popular activation method is to use light induced acyl transfer to create an intermediate reactive towards nucleophile groups, which after the reaction forms a covalent bond between the molecules. The interest of using light to activate the molecules is motivated by our excellent control over light, which is much more precise in both space and time compared to any other mechanism.

The general reaction scheme for light activated N-acyl-5-bromo-7-indoline (Bni) is shown in Scheme 6.1. When illuminated with ~360-380 nm light, the acyl group in the molecule is transferred to the nitro group of the molecule to produce a reactive intermediate. This intermediate has two different path ways: if there are nucleophiles in the solution, the nucleophilic attack on the reactive intermediate creates a new bond between the attacking nucleophile and the acyl group. The reactive intermediate can also self-dissociate into the indoline group and a group with acyl, as shown in path b in Scheme 8.1.⁶⁹ The mechanism has been successfully utilized in making caged molecules with the neurotransmitter L-glutamate, which is inactive when bound to the indoline molecules, but released by photolysis.^{70,71}



Scheme 6.1. Two path ways of indoline molecules after light activation.

Photoactivable molecules are especially interesting for light induced patterning of the surface. Compared with general microarrays where spot sizes are in tens of microns,⁷² photo activation can

produce spots as small as the diffraction limit. Several different strategies for photo functionalization of the surface have been invented. Using Bni for surface patterning, the R group is substituted by an alkanethiol allows the Bni molecules to form a self-assembled monolayer on the gold surface. Biomolecules, such as biotin, with a primary amine terminal can function as a nucleophile that reacts with the acyl group to be covalently bound to the acyl group on the surface. Water molecules promote the self-dissociation of the indoline molecule (path b), and should be avoided for high yield of surface functionalization.⁶⁹ Solvents with nucleophiles may compete with the biotin amine functionalization and should therefore also be avoided.

Chapter 7 Summary of appended papers and outlook

Paper I Ultrahigh sensitivity made simple: nanoplasmonic label-free biosensing with an extremely low limit-of-detection for bacterial and cancer diagnostics

We used HCL to produce samples and performed biosensing experiments in an extinction setup consisting of only a lamp and a miniature spectrometer. Using this setup, we performed label free measurements of antibody and antigen interactions for two clinically relevant biomarkers, namely prostate specific antigen, a biomarker for prostate cancer and extracellular adherence protein, a potential biomarker for *Staphylococcus aureus*. The nanoparticle substrate had high extinction coefficient, resulting in a noise level in the peak position determination below 10^{-4} nm. We could potentially detect as little as $20\text{pg}/\text{cm}^2$ protein binding to the surface.

Paper II: Refractometric Sensing Using Propagating versus Localized Surface Plasmons: A Direct Comparison

In this paper, we compared SPR and LSPR sensing performed under exactly same experimental conditions, in terms of liquid handling, molecular interactions, light sources and detectors. SPR was excited in the Kretschmann configuration via a prism and the LSPR was excited in transmission and scattering mode. We found that the sensitivity of the two methods were very similar, despite one magnitude larger bulk refractive index sensitivity and figure of merit for SPR compared to LSPR. The explanation to this is that the sensing volume for the LSPR is much better matched to the biomolecules than in the SPR case.

Paper III: High-Resolution Microspectroscopy of Plasmonic Nanostructures for Miniaturized Biosensing

In this paper, the probed surface of the particle substrate is greatly reduced and the extinction measurement is performed in a microscope without losing much performance. The minimum number probed particles can be reduced to ~ 250 with maintained short-time noise level. A detailed discussion of when extinction is more favorable than dark field measurements is also included in the article.

Paper IV: Plasmon-enhanced Colorimetric ELISA with Single Molecule Sensitivity

In this paper, we used a single particle LSPR assay that utilizes enzymatic signal amplification of horse radish peroxidase in order to increase the peak shift from a single protein by producing a precipitate around the particle. In order to study peak shifts from many particles at the same time, a liquid crystal tunable filter was used to achieve single particle spectral imaging. Scattering

spectra of up to 100 individual particles were obtained simultaneously. We achieved a sensitivity as low as only a few molecules per particle for multiple individual nanoparticles, which may pave the way for diagnostic applications.

Paper V: Towards Plasmonic Biosensors Functionalized by a Photo-Induced Surface Reaction

We used nitroindoline based photoactivable molecules to form a self assembled monolayer on the gold surface of a nanoplasmonic sensor and a quartz crystal microbalance (QCM) sensor. Using biotin amine together with UV excitation, we successfully functionalized the biotin moiety on both of the sensor surfaces. This may pave the way for localized photofunctionalization that is highly compatible with nanoplasmonic sensors.

Paper VI: ELISA enhanced LSPR sensing on large arrays of single particles prepared by electron beam lithography

In this paper, we characterized the ELISA enhanced LSPR sensing in depth by using a large array of single particles prepared by electron beam lithography. Up to 700 different particles could be evenly placed on the substrate and studied simultaneously. We characterized the particle's bulk refractive index sensitivity variation and the sensitivity distributions on individual particles. The HRP induced precipitates were also studied by TEM and AFM to verify the size and the shape of the particle. We analyzed our results based on the new information and we also discussed a possible way to achieve digital responses from single molecules.

Future works

Further understanding of the HRP precipitation reaction is essential for optimizing the ELISA enhanced plasmonic sensors, therefore more studies on the formations of the precipitation and their morphologies are required. If the background of the precipitation can be reduced, this will be interesting for both ELISA enhanced plasmonic sensors and for the large community of researchers that are studying molecular localization in cells with HRP induced precipitations.

In my measurements only streptavidin and biotin interactions were studied. If antibody and antigens were used, the extra distance between the particle surface and the enzyme will reduce the responses. Thoughtful optimization is required because on one hand a confined field increases the responses close to the surface but if the precipitation happens at a distance from the sensor surface, the confined field may not extend far enough.

In order for the ELISA enhanced plasmonic sensor to achieve a broader impact, we still need to show that this technique can conceptually outperform the ordinary colorimetric ELISA in a 96 well plate with the same antibody and antigen pair. The advantage of LSPR in this case is that they are fully compatible with most of the ELISA plate reader that are based on transmission measurement.

The photo-functionalization strategy that I have investigated in this thesis is a possible tool for localized functionalization of a single or multiple particles, thereby realizing the maximal miniaturization of a multiplexed sensor. However, in order to realize this goal, non specific binding of the proteins needs to be further reduced.

Hyperspectral imaging of LSPR particles have proven to be a very interesting technique to obtain a statistically significant number of signals from independent sensors. However the drawback of this technique is the slow scan rate that limits the possibility to follow the kinetics on the surface of the particle in real time. One way to improving the scan rate is by decreasing the number of data points that construct a spectrum. A study of how the scan rate affects the signal to noise ratio is required to answer the question how fast we can measure. Utilizing this miniaturized sensor arrays, may also enable us to study the local distribution of the molecules i.e. close to a living cell in a label free fashion. This can potentially give us new interesting information about how the cell interacts with its surroundings.

In conclusion, the single LSPR sensor array combined with the hyperspectral imaging technique is an interesting new measurement methodology which potential has not been entirely realized yet.

Acknowledgements

I wish to gratefully and sincerely thank Professor Mikael Käll for all the support and patient guidance since I started in your group. I enjoyed the free rein when working in this group. I am also glad for the steering towards the correct direction when it is required. I am thankful for the wisdoms and advices that you have shared which I will value and cherish throughout the years.

I would like to express my gratitude to Linda Gunnarson who supervised me in my first year as a PhD student and Professor Richard van Duyne for allowing me to visit his lab at Northwestern University. I really enjoy the short time I spend at Northwestern University.

Being in such a creative group is what is most valuable for me. I really enjoyed working with all of my colleagues and collaborators. Andreas, you may not know, but you are my idol and I hope I may follow your foot step one day. Timur, I really enjoy our conversations, you are a source of inspiration for me. Sasha, it is a pleasure to know you and thank you for teaching me HCL. Kasper and Tina, thank you for a fruitful collaboration, I wish I can go further with this photo-functionalization project, maybe something for the next collaboration. Tomasz, thank you for helping me with simulations, I wouldn't be able to finish the last manuscript without your help. I hope we can continue with such efficient collaboration. Vladimir, nothing will be the same again when you leave the group, I wish you all the success at your new workplace. Sorry I never had time to show you AFM. Kristofer, thank you for helping me with the microscope from time to time, thank you for keep our lab in such a good order, I have never noticed that we share the lab together. Mike, I don't know how my PhD would be without your friendship and our discussions. It is through our discussions that most of the ideas were born.

I thank all my friends in Bionanophotonic group: Yurui, Gülis, Kristof, Anni, Robin, Virginia Björn for the great times I have had.

For those to who deserve my *deepest* gratitude and appreciation, my family, you already have my warmest love.

References

1. Liu, Z.; Searson, P. C., Single Nanoporous Gold Nanowire Sensors. *J. Phys. Chem. B* **2006**, *110*, 4318-4322.
2. Kurosawa, S.; Nakamura, M.; Park, J.-W.; Aizawa, H.; Yamada, K.; Hirata, M., Evaluation of a high-affinity QCM immunosensor using antibody fragmentation and 2-methacryloyloxyethyl phosphorylcholine (MPC) polymer. *Biosens Bioelectron* **2004**, *20*, 1134-1139.
3. Wu, G.; Datar, R. H.; Hansen, K. M.; Thundat, T.; Cote, R. J.; Majumdar, A., Bioassay of prostate-specific antigen (PSA) using microcantilevers. *Nat Biotech* **2001**, *19*, 856-860.
4. Lee, J. H.; Hwang, K. S.; Park, J.; Yoon, K. H.; Yoon, D. S.; Kim, T. S., Immunoassay of prostate-specific antigen (PSA) using resonant frequency shift of piezoelectric nanomechanical microcantilever. *Biosens Bioelectron* **2005**, *20*, 2157-2162.
5. Liu, L.; Chen, Y.-y.; Meng, Y.-h.; Chen, S.; Jin, G., Improvement for sensitivity of biosensor with total internal reflection imaging ellipsometry (TIRIE). *Thin Solid Films* **2011**, *519*, 2758-2762.
6. Neumann, T.; Junker, H.-D.; Schmidt, K.; Sekul, R., SPR-based fragment screening: Advantages and applications. *Cur Top Med Che* **2007**, *7*, 1630.
7. Guidi, A.; Laricchia-Robbio, L.; Gianfaldoni, D.; Revoltella, R.; Del Bono, G., Comparison of a conventional immunoassay (ELISA) with a surface plasmon resonance-based biosensor for IGF-1 detection in cows' milk. *Biosens and Bioelectron* **2001**, *16*, 971-977.
8. Chen, S.; et al., Ultrahigh sensitivity made simple: nanoplasmonic label-free biosensing with an extremely low limit-of-detection for bacterial and cancer diagnostics. *Nanotechnology* **2009**, *20*, 434015.
9. Liedberg, B.; Nylander, C.; Lunström, I., Surface plasmon resonance for gas detection and biosensing. *Sensor and Actuator* **1983**, *4*, 299-304.
10. Nylander, C.; Liedberg, B.; Lind, T., Gas detection by means of surface plasmon resonance. *Sensor and Actuator* **1982**, *3*, 79-88.
11. Englebienne, P., Use of colloidal gold surface plasmon resonance peak shift to infer affinity constants from the interactions between protein antigens and antibodies specific for single or multiple epitopes. *Analyst* **1998**, *123*, 1599-1603.
12. Mozsolits, H.; Thomas, W. G.; Aguilar, M.-I., Surface Plasmon Resonance Spectroscopy in the Study of Membrane-Mediated Cell Signalling. *J. Peptide Sci.* **2003**, *9*.
13. Rodríguez-Lorenzo, L.; de la Rica, R.; Álvarez-Puebla, R. n. A.; Liz-Marzán, L. M.; Stevens, M. M., Plasmonic nanosensors with inverse sensitivity by means of enzyme-guided crystal growth. *Nat Mater* **2012**, *11*, 604-607.
14. Sheehan, P. E.; Whitman, L. J., Detection Limits for Nanoscale Biosensors. *Nano Lett.* **2005**, *5*, 803-807.
15. Squires, T. M.; Messenger, R. J.; Manalis, S. R., Making it stick: convection, reaction and diffusion in surface-based biosensors. *Nat Biotech* **2008**, *26*, 417-426.
16. Johnsson, P. B.; Christy, R. W., Optical constants of noble metals. *Phys. Rev. B.* **1972**, *6*, 4370.
17. Palik, E., *Handbook of Optical Constants of Solids*. Academic Press: New York, 1985.
18. Novotny, L.; Hecht, B., *Principles of nano-optics*. Cambridge University Press: 2006.
19. Lindfors, K.; Kalkbrenner, T.; Stoller, P.; Sandoghdar, V., Detection and Spectroscopy of Gold Nanoparticles Using Supercontinuum White Light Confocal Microscopy. *Physical Review Letters* **2004**, *93*, 037401.
20. Xu, H.; Bjerneld, E. J.; Käll, M.; Börjesson, L., Spectroscopy of Single Hemoglobin Molecules by Surface Enhanced Raman Scattering. *Physical Review Letters* **1999**, *83*, 4357-4360.

21. Aćimović, S. S.; Kreuzer, M. P.; González, M. U.; Quidant, R., Plasmon Near-Field Coupling in Metal Dimers as a Step toward Single-Molecule Sensing. *ACS Nano* **2009**, *3*, 1231-1237.
22. Svedendahl, M.; Chen, S.; Dmitriev, A.; Käll, M., Refractometric Sensing Using Propagating versus Localized Surface Plasmons: A Direct Comparison. *Nano Lett.* **2009**, *9*, 4428-4433.
23. Haes, A. J.; Van Duyne, R. P., A Nanoscale Optical Biosensor: Sensitivity and Selectivity of an Approach Based on the Localized Surface Plasmon Resonance Spectroscopy of Triangular Silver Nanoparticles. *J. Am. Chem. Soc.* **2002**, *124*, 10596-10604.
24. Vörös, J., The Density and Refractive Index of Adsorbing Protein Layers. *Biophys. j.* **2004**, *87*, 553-561.
25. Hall, W. P.; Ngatia, S. N.; Van Duyne, R. P., LSPR Biosensor Signal Enhancement Using Nanoparticle–Antibody Conjugates. *The Journal of Physical Chemistry C* **2011**, *115*, 1410-1414.
26. Hall, W. P.; Anker, J. N.; Lin, Y.; Modica, J.; Mrksich, M.; Van Duyne, R. P., A Calcium-Modulated Plasmonic Switch. *Journal of the American Chemical Society* **2008**, *130*, 5836-5837.
27. Jain, P. K.; Huang, W. Y.; El-Sayed, M. A., On the universal scaling behavior of the distance decay of plasmon coupling in metal nanoparticle pairs: A plasmon ruler equation. *Nano Lett.* **2007**, *7*, 2080-2088.
28. Antosiewicz, T. J.; Apell, S. P.; Claudio, V.; Käll, M., A simple model for the resonance shift of localized plasmons due to dielectric particle adhesion. *Opt. Express* **2012**, *20*, 524-533.
29. Ament, I.; Prasad, J.; Henkel, A.; Schmachtel, S.; Sönnichsen, C., Single Unlabeled Protein Detection on Individual Plasmonic Nanoparticles. *Nano Lett.* **2012**, *12*, 1092-1095.
30. Kathryn, M. M.; Hao, F.; Lee, S.; Nordlander, P.; Hafner, J. H., A single molecule immunoassay by localized surface plasmon resonance. *Nanotechnology* **2010**, *21*, 255503.
31. Raschke, G.; Kowarik, S.; Franzl, T.; Sönnichsen, C.; Klar, T. A.; Feldmann, J.; Nichtl, A.; Kürzinger, K., Biomolecular Recognition Based on Single Gold Nanoparticle Light Scattering. *Nano Lett.* **2003**, *3*, 935-938.
32. Baciú, C. L.; Becker, J.; Janshoff, A.; Sönnichsen, C., Protein–Membrane Interaction Probed by Single Plasmonic Nanoparticles. *Nano Lett.* **2008**, *8*, 1724-1728.
33. Zijlstra, P.; Paulo, P. M. R.; Orrit, M., Optical detection of single non-absorbing molecules using the surface plasmon resonance of a gold nanorod. *Nat Nano.* **2012**, *7*, 379-382
34. Haynes, C. L.; Van Duyne, R. P., Nanosphere Lithography: A Versatile Nanofabrication Tool for Studies of Size-Dependent Nanoparticle Optics. *J. of Phys. I Chem. B* **2001**, *105*, 5599-5611.
35. Fredriksson, H.; Alaverdyan, Y.; Dmitriev, A.; Langhammer, C.; Sutherland, D. S.; Zäch, M.; Kasemo, B., Hole-Mask Colloidal Lithography. *Adv. Mater.* **2007**, *19*, 4297-4302.
36. Larsson, E. M.; Alegret, J.; Käll, M.; Sutherland, D. S., Sensing Characteristics of NIR Localized Surface Plasmon Resonances in Gold Nanorings for Application as Ultrasensitive Biosensors. *Nano Lett.* **2007**, *7*, 1256-1263.
37. Haynes, C. L.; McFarland, A. D.; Zhao, L.; Van Duyne, R. P.; Schatz, G. C.; Gunnarsson, L.; Prikulis, J.; Kasemo, B.; Käll, M., Nanoparticle Optics: The Importance of Radiative Dipole Coupling in Two-Dimensional Nanoparticle Arrays. *J. Phys. Chem. B* **2003**, *107*, 7337-7342.
38. Lee, S.-W.; Lee, K.-S.; Ahn, J.; Lee, J.-J.; Kim, M.-G.; Shin, Y.-B., Highly Sensitive Biosensing Using Arrays of Plasmonic Au Nanodisks Realized by Nanoimprint Lithography. *ACS Nano* **2011**, 897–904.
39. Chen, Y.; Munechika, K.; Ginger, D. S., Dependence of Fluorescence Intensity on the Spectral Overlap between Fluorophores and Plasmon Resonant Single Silver Nanoparticles. *Nano Lett.* **2007**, *7*, 690-696.
40. Sönnichsen, C.; Reinhard, B. M.; Liphardt, J.; Alivisatos, A. P., A molecular ruler based on plasmon coupling of single gold and silver nanoparticles. *Nat Biotech* **2005**, *23*, 741

41. Raphael, Marc P.; Christodoulides, Joseph A.; Delehanty, James B.; Long, James P.; Pehrsson, Pehr E.; Byers, Jeff M., Quantitative LSPR Imaging for Biosensing with Single Nanostructure Resolution. *Biophysical journal* **2013**, *104*, 30-36.
42. Raphael, M. P.; Christodoulides, J. A.; Mulvaney, S. P.; Miller, M. M.; Long, J. P.; Byers, J. M., A New Methodology for Quantitative LSPR Biosensing and Imaging. *Analytical Chemistry* **2011**, *84*, 1367-1373.
43. Chen, K. H.; Hogley, J.; Foo, Y. L.; Su, X., Wide-field single metal nanoparticle spectroscopy for high throughput localized surface plasmon resonance sensing. *Lab on a Chip* **2011**, *11*, 1895-1901.
44. Slawson, R.; Ninkov, Z.; Horch, E., Hyperspectral imaging: wide-area spectrophotometry using a liquid-crystal tunable filter. *Publications of the Astronomical Society of the Pacific* **1999**, 621-626.
45. Kopp, G. A., Tunable birefringent filters using liquid crystal variable retarders. **1994**, 193-201.
46. Bingham, J. M.; Willets, K. A.; Shah, N. C.; Andrews, D. Q.; Van Duyne, R. P., Localized Surface Plasmon Resonance Imaging: Simultaneous Single Nanoparticle Spectroscopy and Diffusional Dynamics. *J. Phys. Chem. C* **2009**, *113*, 16839-16842.
47. NC, V., Horseradish peroxidase: a modern view of a classic enzyme. *Phytochemistry* **2004**, *64*, 249-59.
48. Kawaoka, A.; Kawamoto, T.; Ohta, H.; Sekine, M.; Takano, M.; Shinmyo, A., Wound-induced expression of horseradish peroxidase. *Plant Cell Reports* **1994**, *13*, 149-154.
49. E, E.; P, P., Enzyme-linked immunosorbent assay (ELISA). Quantitative assay of immunoglobulin G. *Immunochemistry* **1971**, *9*, 4.
50. Graham, R. C., JR.; Karnovsky, M. J., The early stages of absorption of injected horseradish peroxidase in the promixal tubules of mouse kidney: Ultrastructural cytochemistry by a new technique. *J. Histochem. Cytochem.* **1966**, *14*, 291-302.
51. Yu, J.; Taylor, K. E.; Zou, H.; Biswas, N.; Bewtra, J. K., Phenol Conversion and Dimeric Intermediates in Horseradish Peroxidase-Catalyzed Phenol Removal from Water. *Environmental Science & Technology* **1994**, *28*, 2154-2160.
52. Nakayama, T.; Amachi, T., Fungal peroxidase: its structure, function, and application. *Journal of Molecular Catalysis B: Enzymatic* **1999**, *6*, 185-198.
53. Kim, M.-G.; Shin, Y.-B.; Jung, J.-M.; Ro, H.-S.; Chung, B. H., Enhanced sensitivity of surface plasmon resonance (SPR) immunoassays using a peroxidase-catalyzed precipitation reaction and its application to a protein microarray. *J. Immunol. Methods* **2005**, *297*, 125-132.
54. Xie, X. S.; Lu, H. P., Single-molecule Enzymology. *J. Biol. Chem* **1999**, *274*, 15967-15970.
55. Lu, H. P.; Xun, L.; Xie, X. S., Single-Molecule Enzymatic Dynamics. *Science* **1998**, *282*, 1877-1882.
56. Ullman, A., Formation and structure of self-assembled Monolayers. *Chem. Rev.* **1996**, *96*, 1533
57. Wang, M.; Liechti, K. M.; Wang, Q.; White, J. M., Self-Assembled Silane Monolayers: Fabrication with Nanoscale Uniformity. *Langmuir* **2005**, *21*, 1848-1857.
58. Seifert, M.; Rinke, M. T.; Galla, H.-J., Characterization of Streptavidin Binding to Biotinylated, Binary Self-Assembled Thiol Monolayers—Influence of Component Ratio and Solvent. *Langmuir* **2010**, *26*, 6386-6393.
59. Green, N. M. N., Avidin and streptavidin. *Methods Enzymol* **1990**, *184*, 51-67.
60. Zhao, S.; Reichert, W. M., Influence of biotin lipid surface density and accessibility on avidin binding to the tip of an optical fiber sensor. *Langmuir* **1992**, *8*, 2785-2791.
61. Roberta, D. A.; Giuseppe, G.; Giuseppe, S., Real-Time Binding Kinetics Monitored with Surface Plasmon Resonance Imaging in a Diffusion-Free Environment. *The Open Spectroscopy Journal* **2008**, *2*, 1-9.
62. Jung, L. S.; Nelson, K. E.; Stayton, P. S.; Campbell, C. T., Binding and Dissociation Kinetics of Wild-Type and Mutant Streptavidins on Mixed Biotin-Containing Alkylthiolate Monolayers. *Langmuir* **2000**, *16*, 9421-9432.

63. Gaster, R. S.; Xu, L.; Han, S.-J.; Wilson, R. J.; Hall, D. A.; Osterfeld, S. J.; Yu, H.; Wang, S. X., Quantification of protein interactions and solution transport using high-density GMR sensor arrays. *Nat Nano*. **2011**, *6*, 314.
64. Srisa-Art, M.; Dyson, E. C.; deMello, A. J.; Edell, J. B., Monitoring of Real-Time Streptavidin–Biotin Binding Kinetics Using Droplet Microfluidics. *Analytical Chemistry* **2008**, *80*, 7063-7067.
65. Haes, A. J.; Van Duyne, R. P., A Nanoscale Optical Biosensor: Sensitivity and Selectivity of an Approach Based on the Localized Surface Plasmon Resonance Spectroscopy of Triangular Silver Nanoparticles. *Journal of the American Chemical Society* **2002**, *124*, 10596-10604.
66. Katsamba, P. S.; Navratilova, I.; Calderon-Cacia, M.; Fan, L.; Thornton, K.; Zhu, M.; Bos, T. V.; Forte, C.; Friend, D.; Laird-Offringa, I.; Tavares, G.; Whatley, J.; Shi, E.; Widom, A.; Lindquist, K. C.; Klakamp, S.; Drake, A.; Bohmann, D.; Roell, M.; Rose, L.; Dorocke, J.; Roth, B.; Luginbühl, B.; Myszka, D. G., Kinetic analysis of a high-affinity antibody/antigen interaction performed by multiple Biacore users. *Analytical Biochemistry* **2006**, *352*, 208-221.
67. Nilebäck, E.; Feuz, L.; Uddenberg, H.; Valiokas, R.; Svedhem, S., Characterization and application of a surface modification designed for QCM-D studies of biotinylated biomolecules. *Biosens. Bioelectron*. **2011**, *28*, 407-413.
68. Z, A.; B, S.; M, Z.; P, B., Kinetics of localized adsorption of colloids particles. *Adv. Colloid Interface Sci* **1994**, *48*.
69. Morrison, J.; Wan, P.; Corrie, J. E. T.; Papageorgiou, G., Mechanisms of photorelease of carboxylic acids from 1-acyl-7-nitroindolines in solutions of varying water content. *Photochemical & Photobiological Sciences* **2002**, *1*, 960-969.
70. Papageorgiou, G.; Ogden, D. C.; Barth, A.; Corrie, J. E. T., Photorelease of Carboxylic Acids from 1-Acyl-7-nitroindolines in Aqueous Solution: Rapid and Efficient Photorelease of L-Glutamate1. *Journal of the American Chemical Society* **1999**, *121*, 6503-6504.
71. Canepari, M.; Nelson, L.; Papageorgiou, G.; Corrie, J. E. T.; Ogden, D., Photochemical and pharmacological evaluation of 7-nitroindolinyl-and 4-methoxy-7-nitroindolinyl-amino acids as novel, fast caged neurotransmitters. *Journal of Neuroscience Methods* **2001**, *112*, 29-42.
72. Dandy, D. S.; Wu, P.; Grainger, D. W., Array feature size influences nucleic acid surface capture in DNA microarrays. *Proceedings of the National Academy of Sciences* **2007**, *104*, 8223-8228.

References

1. Liu, Z.; Searson, P. C., Single Nanoporous Gold Nanowire Sensors. *J. Phys. Chem. B* **2006**, *110*, 4318-4322.
2. Kurosawa, S.; Nakamura, M.; Park, J.-W.; Aizawa, H.; Yamada, K.; Hirata, M., Evaluation of a high-affinity QCM immunosensor using antibody fragmentation and 2-methacryloyloxyethyl phosphorylcholine (MPC) polymer. *Biosens Bioelectron* **2004**, *20*, 1134-1139.
3. Wu, G.; Datar, R. H.; Hansen, K. M.; Thundat, T.; Cote, R. J.; Majumdar, A., Bioassay of prostate-specific antigen (PSA) using microcantilevers. *Nat Biotech* **2001**, *19*, 856-860.
4. Lee, J. H.; Hwang, K. S.; Park, J.; Yoon, K. H.; Yoon, D. S.; Kim, T. S., Immunoassay of prostate-specific antigen (PSA) using resonant frequency shift of piezoelectric nanomechanical microcantilever. *Biosens Bioelectron* **2005**, *20*, 2157-2162.
5. Liu, L.; Chen, Y.-y.; Meng, Y.-h.; Chen, S.; Jin, G., Improvement for sensitivity of biosensor with total internal reflection imaging ellipsometry (TIRIE). *Thin Solid Films* **2011**, *519*, 2758-2762.
6. Neumann, T.; Junker, H.-D.; Schmidt, K.; Sekul, R., SPR-based fragment screening: Advantages and applications. *Cur Top Med Che* **2007**, *7*, 1630.
7. Guidi, A.; Laricchia-Robbio, L.; Gianfaldoni, D.; Revoltella, R.; Del Bono, G., Comparison of a conventional immunoassay (ELISA) with a surface plasmon resonance-based biosensor for IGF-1 detection in cows' milk. *Biosens and Bioelectron* **2001**, *16*, 971-977.
8. Chen, S.; et al., Ultrahigh sensitivity made simple: nanoplasmonic label-free biosensing with an extremely low limit-of-detection for bacterial and cancer diagnostics. *Nanotechnology* **2009**, *20*, 434015.
9. Liedberg, B.; Nylander, C.; Lunström, I., Surface plasmon resonance for gas detection and biosensing. *Sensor and Actuator* **1983**, *4*, 299-304.
10. Nylander, C.; Liedberg, B.; Lind, T., Gas detection by means of surface plasmon resonance. *Sensor and Actuator* **1982**, *3*, 79-88.
11. Englebienne, P., Use of colloidal gold surface plasmon resonance peak shift to infer affinity constants from the interactions between protein antigens and antibodies specific for single or multiple epitopes. *Analyst* **1998**, *123*, 1599-1603.
12. Mozsolits, H.; Thomas, W. G.; Aguilar, M.-I., Surface Plasmon Resonance Spectroscopy in the Study of Membrane-Mediated Cell Signalling. *J. Peptide Sci.* **2003**, *9*.
13. Rodríguez-Lorenzo, L.; de la Rica, R.; Álvarez-Puebla, R. n. A.; Liz-Marzán, L. M.; Stevens, M. M., Plasmonic nanosensors with inverse sensitivity by means of enzyme-guided crystal growth. *Nat Mater* **2012**, *11*, 604-607.
14. Sheehan, P. E.; Whitman, L. J., Detection Limits for Nanoscale Biosensors. *Nano Lett.* **2005**, *5*, 803-807.
15. Squires, T. M.; Messinger, R. J.; Manalis, S. R., Making it stick: convection, reaction and diffusion in surface-based biosensors. *Nat Biotech* **2008**, *26*, 417-426.
16. Johansson, P. B.; Christy, R. W., Optical constants of noble metals. *Phys. Rev. B.* **1972**, *6*, 4370.
17. Palik, E., *Handbook of Optical Constants of Solids*. Academic Press: New York, 1985.
18. Novotny, L.; Hecht, B., *Principles of nano-optics*. Cambridge University Press: 2006.
19. Lindfors, K.; Kalkbrenner, T.; Stoller, P.; Sandoghdar, V., Detection and Spectroscopy of Gold Nanoparticles Using Supercontinuum White Light Confocal Microscopy. *Physical Review Letters* **2004**, *93*, 037401.
20. Xu, H.; Bjerneld, E. J.; Käll, M.; Börjesson, L., Spectroscopy of Single Hemoglobin Molecules by Surface Enhanced Raman Scattering. *Physical Review Letters* **1999**, *83*, 4357-4360.

21. Aćimović, S. S.; Kreuzer, M. P.; González, M. U.; Quidant, R., Plasmon Near-Field Coupling in Metal Dimers as a Step toward Single-Molecule Sensing. *ACS Nano* **2009**, *3*, 1231-1237.
22. Svedendahl, M.; Chen, S.; Dmitriev, A.; Käll, M., Refractometric Sensing Using Propagating versus Localized Surface Plasmons: A Direct Comparison. *Nano Lett.* **2009**, *9*, 4428-4433.
23. Haes, A. J.; Van Duyne, R. P., A Nanoscale Optical Biosensor: Sensitivity and Selectivity of an Approach Based on the Localized Surface Plasmon Resonance Spectroscopy of Triangular Silver Nanoparticles. *J. Am. Chem. Soc.* **2002**, *124*, 10596-10604.
24. Vörös, J., The Density and Refractive Index of Adsorbing Protein Layers. *Biophys. j.* **2004**, *87*, 553-561.
25. Hall, W. P.; Ngatia, S. N.; Van Duyne, R. P., LSPR Biosensor Signal Enhancement Using Nanoparticle–Antibody Conjugates. *The Journal of Physical Chemistry C* **2011**, *115*, 1410-1414.
26. Hall, W. P.; Anker, J. N.; Lin, Y.; Modica, J.; Mrksich, M.; Van Duyne, R. P., A Calcium-Modulated Plasmonic Switch. *Journal of the American Chemical Society* **2008**, *130*, 5836-5837.
27. Jain, P. K.; Huang, W. Y.; El-Sayed, M. A., On the universal scaling behavior of the distance decay of plasmon coupling in metal nanoparticle pairs: A plasmon ruler equation. *Nano Lett.* **2007**, *7*, 2080-2088.
28. Antosiewicz, T. J.; Apell, S. P.; Claudio, V.; Käll, M., A simple model for the resonance shift of localized plasmons due to dielectric particle adhesion. *Opt. Express* **2012**, *20*, 524-533.
29. Ament, I.; Prasad, J.; Henkel, A.; Schmachtel, S.; Sönnichsen, C., Single Unlabeled Protein Detection on Individual Plasmonic Nanoparticles. *Nano Lett.* **2012**, *12*, 1092-1095.
30. Kathryn, M. M.; Hao, F.; Lee, S.; Nordlander, P.; Hafner, J. H., A single molecule immunoassay by localized surface plasmon resonance. *Nanotechnology* **2010**, *21*, 255503.
31. Raschke, G.; Kowarik, S.; Franzl, T.; Sönnichsen, C.; Klar, T. A.; Feldmann, J.; Nichtl, A.; Kürzinger, K., Biomolecular Recognition Based on Single Gold Nanoparticle Light Scattering. *Nano Lett.* **2003**, *3*, 935-938.
32. Baciú, C. L.; Becker, J.; Janshoff, A.; Sönnichsen, C., Protein–Membrane Interaction Probed by Single Plasmonic Nanoparticles. *Nano Lett.* **2008**, *8*, 1724-1728.
33. Zijlstra, P.; Paulo, P. M. R.; Orrit, M., Optical detection of single non-absorbing molecules using the surface plasmon resonance of a gold nanorod. *Nat Nano.* **2012**, *7*, 379-382
34. Haynes, C. L.; Van Duyne, R. P., Nanosphere Lithography: A Versatile Nanofabrication Tool for Studies of Size-Dependent Nanoparticle Optics. *J. of Phys. Chem. B* **2001**, *105*, 5599-5611.
35. Fredriksson, H.; Alaverdyan, Y.; Dmitriev, A.; Langhammer, C.; Sutherland, D. S.; Zäch, M.; Kasemo, B., Hole-Mask Colloidal Lithography. *Adv. Mater.* **2007**, *19*, 4297-4302.
36. Larsson, E. M.; Alegret, J.; Käll, M.; Sutherland, D. S., Sensing Characteristics of NIR Localized Surface Plasmon Resonances in Gold Nanorings for Application as Ultrasensitive Biosensors. *Nano Lett.* **2007**, *7*, 1256-1263.
37. Haynes, C. L.; McFarland, A. D.; Zhao, L.; Van Duyne, R. P.; Schatz, G. C.; Gunnarsson, L.; Prikulis, J.; Kasemo, B.; Käll, M., Nanoparticle Optics: The Importance of Radiative Dipole Coupling in Two-Dimensional Nanoparticle Arrays. *J. Phys. Chem. B* **2003**, *107*, 7337-7342.
38. Lee, S.-W.; Lee, K.-S.; Ahn, J.; Lee, J.-J.; Kim, M.-G.; Shin, Y.-B., Highly Sensitive Biosensing Using Arrays of Plasmonic Au Nanodisks Realized by Nanoimprint Lithography. *ACS Nano* **2011**, 897–904.
39. Chen, Y.; Munechika, K.; Ginger, D. S., Dependence of Fluorescence Intensity on the Spectral Overlap between Fluorophores and Plasmon Resonant Single Silver Nanoparticles. *Nano Lett.* **2007**, *7*, 690-696.
40. Sönnichsen, C.; Reinhard, B. M.; Liphardt, J.; Alivisatos, A. P., A molecular ruler based on plasmon coupling of single gold and silver nanoparticles. *Nat Biotech* **2005**, *23*, 741

41. Raphael, Marc P.; Christodoulides, Joseph A.; Delehanty, James B.; Long, James P.; Pehrsson, Pehr E.; Byers, Jeff M., Quantitative LSPR Imaging for Biosensing with Single Nanostructure Resolution. *Biophysical journal* **2013**, *104*, 30-36.
42. Raphael, M. P.; Christodoulides, J. A.; Mulvaney, S. P.; Miller, M. M.; Long, J. P.; Byers, J. M., A New Methodology for Quantitative LSPR Biosensing and Imaging. *Analytical Chemistry* **2011**, *84*, 1367-1373.
43. Chen, K. H.; Hogley, J.; Foo, Y. L.; Su, X., Wide-field single metal nanoparticle spectroscopy for high throughput localized surface plasmon resonance sensing. *Lab on a Chip* **2011**, *11*, 1895-1901.
44. Slawson, R.; Ninkov, Z.; Horch, E., Hyperspectral imaging: wide-area spectrophotometry using a liquid-crystal tunable filter. *Publications of the Astronomical Society of the Pacific* **1999**, 621-626.
45. Kopp, G. A., Tunable birefringent filters using liquid crystal variable retarders. **1994**, 193-201.
46. Bingham, J. M.; Willets, K. A.; Shah, N. C.; Andrews, D. Q.; Van Duyne, R. P., Localized Surface Plasmon Resonance Imaging: Simultaneous Single Nanoparticle Spectroscopy and Diffusional Dynamics. *J. Phys. Chem. C* **2009**, *113*, 16839-16842.
47. NC, V., Horseradish peroxidase: a modern view of a classic enzyme. *Phytochemistry* **2004**, *64*, 249-59.
48. Kawaoka, A.; Kawamoto, T.; Ohta, H.; Sekine, M.; Takano, M.; Shinmyo, A., Wound-induced expression of horseradish peroxidase. *Plant Cell Reports* **1994**, *13*, 149-154.
49. E, E.; P, P., Enzyme-linked immunosorbent assay (ELISA). Quantitative assay of immunoglobulin G. *Immunochemistry* **1971**, *9*, 4.
50. Graham, R. C., JR.; Karnovsky, M. J., The early stages of absorption of injected horseradish peroxidase in the promixal tubules of mouse kidney: Ultrastructural cytochemistry by a new technique. *J. Histochem. Cytochem.* **1966**, *14*, 291-302.
51. Yu, J.; Taylor, K. E.; Zou, H.; Biswas, N.; Bewtra, J. K., Phenol Conversion and Dimeric Intermediates in Horseradish Peroxidase-Catalyzed Phenol Removal from Water. *Environmental Science & Technology* **1994**, *28*, 2154-2160.
52. Nakayama, T.; Amachi, T., Fungal peroxidase: its structure, function, and application. *Journal of Molecular Catalysis B: Enzymatic* **1999**, *6*, 185-198.
53. Kim, M.-G.; Shin, Y.-B.; Jung, J.-M.; Ro, H.-S.; Chung, B. H., Enhanced sensitivity of surface plasmon resonance (SPR) immunoassays using a peroxidase-catalyzed precipitation reaction and its application to a protein microarray. *J. Immunol. Methods* **2005**, *297*, 125-132.
54. Xie, X. S.; Lu, H. P., Single-molecule Enzymology. *J. Biol. Chem* **1999**, *274*, 15967-15970.
55. Lu, H. P.; Xun, L.; Xie, X. S., Single-Molecule Enzymatic Dynamics. *Science* **1998**, *282*, 1877-1882.
56. Ullman, A., Formation and structure of self-assembled Monolayers. *Chem. Rev.* **1996**, *96*, 1533
57. Wang, M.; Liechti, K. M.; Wang, Q.; White, J. M., Self-Assembled Silane Monolayers: Fabrication with Nanoscale Uniformity. *Langmuir* **2005**, *21*, 1848-1857.
58. Seifert, M.; Rinke, M. T.; Galla, H.-J., Characterization of Streptavidin Binding to Biotinylated, Binary Self-Assembled Thiol Monolayers—Influence of Component Ratio and Solvent. *Langmuir* **2010**, *26*, 6386-6393.
59. Green, N. M. N., Avidin and streptavidin. *Methods Enzymol* **1990**, *184*, 51-67.
60. Zhao, S.; Reichert, W. M., Influence of biotin lipid surface density and accessibility on avidin binding to the tip of an optical fiber sensor. *Langmuir* **1992**, *8*, 2785-2791.
61. Roberta, D. A.; Giuseppe, G.; Giuseppe, S., Real-Time Binding Kinetics Monitored with Surface Plasmon Resonance Imaging in a Diffusion-Free Environment. *The Open Spectroscopy Journal* **2008**, *2*, 1-9.
62. Jung, L. S.; Nelson, K. E.; Stayton, P. S.; Campbell, C. T., Binding and Dissociation Kinetics of Wild-Type and Mutant Streptavidins on Mixed Biotin-Containing Alkylthiolate Monolayers. *Langmuir* **2000**, *16*, 9421-9432.

63. Gaster, R. S.; Xu, L.; Han, S.-J.; Wilson, R. J.; Hall, D. A.; Osterfeld, S. J.; Yu, H.; Wang, S. X., Quantification of protein interactions and solution transport using high-density GMR sensor arrays. *Nat Nano*. **2011**, *6*, 314.
64. Srisa-Art, M.; Dyson, E. C.; deMello, A. J.; Edell, J. B., Monitoring of Real-Time Streptavidin–Biotin Binding Kinetics Using Droplet Microfluidics. *Analytical Chemistry* **2008**, *80*, 7063-7067.
65. Haes, A. J.; Van Duyne, R. P., A Nanoscale Optical Biosensor: Sensitivity and Selectivity of an Approach Based on the Localized Surface Plasmon Resonance Spectroscopy of Triangular Silver Nanoparticles. *Journal of the American Chemical Society* **2002**, *124*, 10596-10604.
66. Katsamba, P. S.; Navratilova, I.; Calderon-Cacia, M.; Fan, L.; Thornton, K.; Zhu, M.; Bos, T. V.; Forte, C.; Friend, D.; Laird-Offringa, I.; Tavares, G.; Whatley, J.; Shi, E.; Widom, A.; Lindquist, K. C.; Klakamp, S.; Drake, A.; Bohmann, D.; Roell, M.; Rose, L.; Dorocke, J.; Roth, B.; Luginbühl, B.; Myszka, D. G., Kinetic analysis of a high-affinity antibody/antigen interaction performed by multiple Biacore users. *Analytical Biochemistry* **2006**, *352*, 208-221.
67. Nilebäck, E.; Feuz, L.; Uddenberg, H.; Valiokas, R.; Svedhem, S., Characterization and application of a surface modification designed for QCM-D studies of biotinylated biomolecules. *Biosens. Bioelectron.* **2011**, *28*, 407-413.
68. Z, A.; B, S.; M, Z.; P, B., Kinetics of localized adsorption of colloids particles. *Adv. Colloid Interface Sci* **1994**, *48*.
69. Morrison, J.; Wan, P.; Corrie, J. E. T.; Papageorgiou, G., Mechanisms of photorelease of carboxylic acids from 1-acyl-7-nitroindolines in solutions of varying water content. *Photochemical & Photobiological Sciences* **2002**, *1*, 960-969.
70. Papageorgiou, G.; Ogden, D. C.; Barth, A.; Corrie, J. E. T., Photorelease of Carboxylic Acids from 1-Acyl-7-nitroindolines in Aqueous Solution: Rapid and Efficient Photorelease of L-Glutamate1. *Journal of the American Chemical Society* **1999**, *121*, 6503-6504.
71. Canepari, M.; Nelson, L.; Papageorgiou, G.; Corrie, J. E. T.; Ogden, D., Photochemical and pharmacological evaluation of 7-nitroindolinyl-and 4-methoxy-7-nitroindolinyl-amino acids as novel, fast caged neurotransmitters. *Journal of Neuroscience Methods* **2001**, *112*, 29-42.
72. Dandy, D. S.; Wu, P.; Grainger, D. W., Array feature size influences nucleic acid surface capture in DNA microarrays. *Proceedings of the National Academy of Sciences* **2007**, *104*, 8223-8228.

References

1. Liu, Z.; Searson, P. C., Single Nanoporous Gold Nanowire Sensors. *J. Phys. Chem. B* **2006**, *110*, 4318-4322.
2. Kurosawa, S.; Nakamura, M.; Park, J.-W.; Aizawa, H.; Yamada, K.; Hirata, M., Evaluation of a high-affinity QCM immunosensor using antibody fragmentation and 2-methacryloyloxyethyl phosphorylcholine (MPC) polymer. *Biosens Bioelectron* **2004**, *20*, 1134-1139.
3. Wu, G.; Datar, R. H.; Hansen, K. M.; Thundat, T.; Cote, R. J.; Majumdar, A., Bioassay of prostate-specific antigen (PSA) using microcantilevers. *Nat Biotech* **2001**, *19*, 856-860.
4. Lee, J. H.; Hwang, K. S.; Park, J.; Yoon, K. H.; Yoon, D. S.; Kim, T. S., Immunoassay of prostate-specific antigen (PSA) using resonant frequency shift of piezoelectric nanomechanical microcantilever. *Biosens Bioelectron* **2005**, *20*, 2157-2162.
5. Liu, L.; Chen, Y.-y.; Meng, Y.-h.; Chen, S.; Jin, G., Improvement for sensitivity of biosensor with total internal reflection imaging ellipsometry (TIRIE). *Thin Solid Films* **2011**, *519*, 2758-2762.
6. Neumann, T.; Junker, H.-D.; Schmidt, K.; Sekul, R., SPR-based fragment screening: Advantages and applications. *Cur Top Med Che* **2007**, *7*, 1630.
7. Guidi, A.; Laricchia-Robbio, L.; Gianfaldoni, D.; Revoltella, R.; Del Bono, G., Comparison of a conventional immunoassay (ELISA) with a surface plasmon resonance-based biosensor for IGF-1 detection in cows' milk. *Biosens and Bioelectron* **2001**, *16*, 971-977.
8. Chen, S.; et al., Ultrahigh sensitivity made simple: nanoplasmonic label-free biosensing with an extremely low limit-of-detection for bacterial and cancer diagnostics. *Nanotechnology* **2009**, *20*, 434015.
9. Liedberg, B.; Nylander, C.; Lunström, I., Surface plasmon resonance for gas detection and biosensing. *Sensor and Actuator* **1983**, *4*, 299-304.
10. Nylander, C.; Liedberg, B.; Lind, T., Gas detection by means of surface plasmon resonance. *Sensor and Actuator* **1982**, *3*, 79-88.
11. Englebienne, P., Use of colloidal gold surface plasmon resonance peak shift to infer affinity constants from the interactions between protein antigens and antibodies specific for single or multiple epitopes. *Analyst* **1998**, *123*, 1599-1603.
12. Mozsolits, H.; Thomas, W. G.; Aguilar, M.-I., Surface Plasmon Resonance Spectroscopy in the Study of Membrane-Mediated Cell Signalling. *J. Peptide Sci.* **2003**, *9*.
13. Rodríguez-Lorenzo, L.; de la Rica, R.; Álvarez-Puebla, R. n. A.; Liz-Marzán, L. M.; Stevens, M. M., Plasmonic nanosensors with inverse sensitivity by means of enzyme-guided crystal growth. *Nat Mater* **2012**, *11*, 604-607.
14. Sheehan, P. E.; Whitman, L. J., Detection Limits for Nanoscale Biosensors. *Nano Lett.* **2005**, *5*, 803-807.
15. Squires, T. M.; Messenger, R. J.; Manalis, S. R., Making it stick: convection, reaction and diffusion in surface-based biosensors. *Nat Biotech* **2008**, *26*, 417-426.
16. Johnsson, P. B.; Christy, R. W., Optical constants of noble metals. *Phys. Rev. B.* **1972**, *6*, 4370.
17. Palik, E., *Handbook of Optical Constants of Solids*. Academic Press: New York, 1985.
18. Novotny, L.; Hecht, B., *Principles of nano-optics*. Cambridge University Press: 2006.
19. Lindfors, K.; Kalkbrenner, T.; Stoller, P.; Sandoghdar, V., Detection and Spectroscopy of Gold Nanoparticles Using Supercontinuum White Light Confocal Microscopy. *Physical Review Letters* **2004**, *93*, 037401.
20. Xu, H.; Bjerneld, E. J.; Käll, M.; Börjesson, L., Spectroscopy of Single Hemoglobin Molecules by Surface Enhanced Raman Scattering. *Physical Review Letters* **1999**, *83*, 4357-4360.

21. Aćimović, S. S.; Kreuzer, M. P.; González, M. U.; Quidant, R., Plasmon Near-Field Coupling in Metal Dimers as a Step toward Single-Molecule Sensing. *ACS Nano* **2009**, *3*, 1231-1237.
22. Svedendahl, M.; Chen, S.; Dmitriev, A.; Käll, M., Refractometric Sensing Using Propagating versus Localized Surface Plasmons: A Direct Comparison. *Nano Lett.* **2009**, *9*, 4428-4433.
23. Haes, A. J.; Van Duyne, R. P., A Nanoscale Optical Biosensor: Sensitivity and Selectivity of an Approach Based on the Localized Surface Plasmon Resonance Spectroscopy of Triangular Silver Nanoparticles. *J. Am. Chem. Soc.* **2002**, *124*, 10596-10604.
24. Vörös, J., The Density and Refractive Index of Adsorbing Protein Layers. *Biophys. j.* **2004**, *87*, 553-561.
25. Hall, W. P.; Ngatia, S. N.; Van Duyne, R. P., LSPR Biosensor Signal Enhancement Using Nanoparticle–Antibody Conjugates. *The Journal of Physical Chemistry C* **2011**, *115*, 1410-1414.
26. Hall, W. P.; Anker, J. N.; Lin, Y.; Modica, J.; Mrksich, M.; Van Duyne, R. P., A Calcium-Modulated Plasmonic Switch. *Journal of the American Chemical Society* **2008**, *130*, 5836-5837.
27. Jain, P. K.; Huang, W. Y.; El-Sayed, M. A., On the universal scaling behavior of the distance decay of plasmon coupling in metal nanoparticle pairs: A plasmon ruler equation. *Nano Lett.* **2007**, *7*, 2080-2088.
28. Antosiewicz, T. J.; Apell, S. P.; Claudio, V.; Käll, M., A simple model for the resonance shift of localized plasmons due to dielectric particle adhesion. *Opt. Express* **2012**, *20*, 524-533.
29. Ament, I.; Prasad, J.; Henkel, A.; Schmachtel, S.; Sönnichsen, C., Single Unlabeled Protein Detection on Individual Plasmonic Nanoparticles. *Nano Lett.* **2012**, *12*, 1092-1095.
30. Kathryn, M. M.; Hao, F.; Lee, S.; Nordlander, P.; Hafner, J. H., A single molecule immunoassay by localized surface plasmon resonance. *Nanotechnology* **2010**, *21*, 255503.
31. Raschke, G.; Kowarik, S.; Franzl, T.; Sönnichsen, C.; Klar, T. A.; Feldmann, J.; Nichtl, A.; Kürzinger, K., Biomolecular Recognition Based on Single Gold Nanoparticle Light Scattering. *Nano Lett.* **2003**, *3*, 935-938.
32. Baciú, C. L.; Becker, J.; Janshoff, A.; Sönnichsen, C., Protein–Membrane Interaction Probed by Single Plasmonic Nanoparticles. *Nano Lett.* **2008**, *8*, 1724-1728.
33. Zijlstra, P.; Paulo, P. M. R.; Orrit, M., Optical detection of single non-absorbing molecules using the surface plasmon resonance of a gold nanorod. *Nat Nano.* **2012**, *7*.
34. Haynes, C. L.; Van Duyne, R. P., Nanosphere Lithography: A Versatile Nanofabrication Tool for Studies of Size-Dependent Nanoparticle Optics. *J. of Phys. Chem. B* **2001**, *105*, 5599-5611.
35. Fredriksson, H.; Alaverdyan, Y.; Dmitriev, A.; Langhammer, C.; Sutherland, D. S.; Zäch, M.; Kasemo, B., Hole-Mask Colloidal Lithography. *Adv. Mater.* **2007**, *19*, 4297-4302.
36. Larsson, E. M.; Alegret, J.; Käll, M.; Sutherland, D. S., Sensing Characteristics of NIR Localized Surface Plasmon Resonances in Gold Nanorings for Application as Ultrasensitive Biosensors. *Nano Lett.* **2007**, *7*, 1256-1263.
37. Haynes, C. L.; McFarland, A. D.; Zhao, L.; Van Duyne, R. P.; Schatz, G. C.; Gunnarsson, L.; Prikulis, J.; Kasemo, B.; Käll, M., Nanoparticle Optics: The Importance of Radiative Dipole Coupling in Two-Dimensional Nanoparticle Arrays. *J. Phys. Chem. B* **2003**, *107*, 7337-7342.
38. Lee, S.-W.; Lee, K.-S.; Ahn, J.; Lee, J.-J.; Kim, M.-G.; Shin, Y.-B., Highly Sensitive Biosensing Using Arrays of Plasmonic Au Nanodisks Realized by Nanoimprint Lithography. *ACS Nano* **2011**, 897–904.
39. Chen, Y.; Munechika, K.; Ginger, D. S., Dependence of Fluorescence Intensity on the Spectral Overlap between Fluorophores and Plasmon Resonant Single Silver Nanoparticles. *Nano Lett.* **2007**, *7*, 690-696.
40. Sönnichsen, C.; Reinhard, B. M.; Liphardt, J.; Alivisatos, A. P., A molecular ruler based on plasmon coupling of single gold and silver nanoparticles. *Nat Biotech* **2005**, *23*.

41. Raphael, Marc P.; Christodoulides, Joseph A.; Delehanty, James B.; Long, James P.; Pehrsson, Pehr E.; Byers, Jeff M., Quantitative LSPR Imaging for Biosensing with Single Nanostructure Resolution. *Biophysical journal* **2013**, *104*, 30-36.
42. Raphael, M. P.; Christodoulides, J. A.; Mulvaney, S. P.; Miller, M. M.; Long, J. P.; Byers, J. M., A New Methodology for Quantitative LSPR Biosensing and Imaging. *Analytical Chemistry* **2011**, *84*, 1367-1373.
43. Chen, K. H.; Hogley, J.; Foo, Y. L.; Su, X., Wide-field single metal nanoparticle spectroscopy for high throughput localized surface plasmon resonance sensing. *Lab on a Chip* **2011**, *11*, 1895-1901.
44. Slawson, R.; Ninkov, Z.; Horch, E., Hyperspectral imaging: wide-area spectrophotometry using a liquid-crystal tunable filter. *Publications of the Astronomical Society of the Pacific* **1999**, 621-626.
45. Kopp, G. A., Tunable birefringent filters using liquid crystal variable retarders. **1994**, 193-201.
46. Bingham, J. M.; Willets, K. A.; Shah, N. C.; Andrews, D. Q.; Van Duyne, R. P., Localized Surface Plasmon Resonance Imaging: Simultaneous Single Nanoparticle Spectroscopy and Diffusional Dynamics. *J. Phys. Chem. C* **2009**, *113*, 16839-16842.
47. NC, V., Horseradish peroxidase: a modern view of a classic enzyme. *Phytochemistry* **2004**, *64*, 249-59.
48. Kawaoka, A.; Kawamoto, T.; Ohta, H.; Sekine, M.; Takano, M.; Shinmyo, A., Wound-induced expression of horseradish peroxidase. *Plant Cell Reports* **1994**, *13*, 149-154.
49. E, E.; P, P., Enzyme-linked immunosorbent assay (ELISA). Quantitative assay of immunoglobulin G. *Immunochemistry* **1971**, *9*, 4.
50. Graham, R. C., JR.; Karnovsky, M. J., The early stages of absorption of injected horseradish peroxidase in the promixal tubules of mouse kidney: Ultrastructural cytochemistry by a new technique. *J. Histochem. Cytochem.* **1966**, *14*, 291-302.
51. Yu, J.; Taylor, K. E.; Zou, H.; Biswas, N.; Bewtra, J. K., Phenol Conversion and Dimeric Intermediates in Horseradish Peroxidase-Catalyzed Phenol Removal from Water. *Environmental Science & Technology* **1994**, *28*, 2154-2160.
52. Nakayama, T.; Amachi, T., Fungal peroxidase: its structure, function, and application. *Journal of Molecular Catalysis B: Enzymatic* **1999**, *6*, 185-198.
53. Kim, M.-G.; Shin, Y.-B.; Jung, J.-M.; Ro, H.-S.; Chung, B. H., Enhanced sensitivity of surface plasmon resonance (SPR) immunoassays using a peroxidase-catalyzed precipitation reaction and its application to a protein microarray. *J. Immunol. Methods* **2005**, *297*, 125-132.
54. Xie, X. S.; Lu, H. P., Single-molecule Enzymology. *J. Biol. Chem* **1999**, *274*, 15967-15970.
55. Lu, H. P.; Xun, L.; Xie, X. S., Single-Molecule Enzymatic Dynamics. *Science* **1998**, *282*, 1877-1882.
56. Ullman, A., Formation and structure of self-assembled Monolayers. *Chem. Rev.* **1996**.
57. Wang, M.; Liechti, K. M.; Wang, Q.; White, J. M., Self-Assembled Silane Monolayers: Fabrication with Nanoscale Uniformity. *Langmuir* **2005**, *21*, 1848-1857.
58. Seifert, M.; Rinke, M. T.; Galla, H.-J., Characterization of Streptavidin Binding to Biotinylated, Binary Self-Assembled Thiol Monolayers—Influence of Component Ratio and Solvent. *Langmuir* **2010**, *26*, 6386-6393.
59. Green, N. M. N., Avidin and streptavidin. *Methods Enzymol* **1990**, *184*, 51-67.
60. Zhao, S.; Reichert, W. M., Influence of biotin lipid surface density and accessibility on avidin binding to the tip of an optical fiber sensor. *Langmuir* **1992**, *8*, 2785-2791.
61. Roberta, D. A.; Giuseppe, G.; Giuseppe, S., Real-Time Binding Kinetics Monitored with Surface Plasmon Resonance Imaging in a Diffusion-Free Environment. *The Open Spectroscopy Journal* **2008**, *2*, 1-9.
62. Jung, L. S.; Nelson, K. E.; Stayton, P. S.; Campbell, C. T., Binding and Dissociation Kinetics of Wild-Type and Mutant Streptavidins on Mixed Biotin-Containing Alkylthiolate Monolayers. *Langmuir* **2000**, *16*, 9421-9432.

63. Gaster, R. S.; Xu, L.; Han, S.-J.; Wilson, R. J.; Hall, D. A.; Osterfeld, S. J.; Yu, H.; Wang, S. X., Quantification of protein interactions and solution transport using high-density GMR sensor arrays. *Nat Nano*. **2011**, *6*, 314.
64. Srisa-Art, M.; Dyson, E. C.; deMello, A. J.; Edell, J. B., Monitoring of Real-Time Streptavidin–Biotin Binding Kinetics Using Droplet Microfluidics. *Analytical Chemistry* **2008**, *80*, 7063-7067.
65. Haes, A. J.; Van Duyne, R. P., A Nanoscale Optical Biosensor: Sensitivity and Selectivity of an Approach Based on the Localized Surface Plasmon Resonance Spectroscopy of Triangular Silver Nanoparticles. *Journal of the American Chemical Society* **2002**, *124*, 10596-10604.
66. Katsamba, P. S.; Navratilova, I.; Calderon-Cacia, M.; Fan, L.; Thornton, K.; Zhu, M.; Bos, T. V.; Forte, C.; Friend, D.; Laird-Offringa, I.; Tavares, G.; Whatley, J.; Shi, E.; Widom, A.; Lindquist, K. C.; Klakamp, S.; Drake, A.; Bohmann, D.; Roell, M.; Rose, L.; Dorocke, J.; Roth, B.; Luginbühl, B.; Myszka, D. G., Kinetic analysis of a high-affinity antibody/antigen interaction performed by multiple Biacore users. *Analytical Biochemistry* **2006**, *352*, 208-221.
67. Nilebäck, E.; Feuz, L.; Uddenberg, H.; Valiokas, R.; Svedhem, S., Characterization and application of a surface modification designed for QCM-D studies of biotinylated biomolecules. *Biosens. Bioelectron*. **2011**, *28*, 407-413.
68. Z, A.; B, S.; M, Z.; P, B., Kinetics of localized adsorption of colloids particles. *Adv. Colloid Interface Sci* **1994**, *48*.
69. Morrison, J.; Wan, P.; Corrie, J. E. T.; Papageorgiou, G., Mechanisms of photorelease of carboxylic acids from 1-acyl-7-nitroindolines in solutions of varying water content. *Photochemical & Photobiological Sciences* **2002**, *1*, 960-969.
70. Papageorgiou, G.; Ogden, D. C.; Barth, A.; Corrie, J. E. T., Photorelease of Carboxylic Acids from 1-Acyl-7-nitroindolines in Aqueous Solution: Rapid and Efficient Photorelease of l-Glutamate1. *Journal of the American Chemical Society* **1999**, *121*, 6503-6504.
71. Canepari, M.; Nelson, L.; Papageorgiou, G.; Corrie, J. E. T.; Ogden, D., Photochemical and pharmacological evaluation of 7-nitroindolinyl-and 4-methoxy-7-nitroindolinyl-amino acids as novel, fast caged neurotransmitters. *Journal of Neuroscience Methods* **2001**, *112*, 29-42.
72. Dandy, D. S.; Wu, P.; Grainger, D. W., Array feature size influences nucleic acid surface capture in DNA microarrays. *Proceedings of the National Academy of Sciences* **2007**, *104*, 8223-8228.